



Invited review

A review of the bipolar see–saw from synchronized and high resolution ice core water stable isotope records from Greenland and East Antarctica



A. Landais^{a,*}, V. Masson-Delmotte^a, B. Stenni^{b,c}, E. Selmo^d, D.M. Roche^{a,e}, J. Jouzel^a, F. Lambert^f, M. Guillevic^{a,h}, L. Bazin^a, O. Arzel^g, B. Vinther^h, V. Gkinis^h, T. Popp^h

^a Laboratoire des Sciences du Climat et de l'Environnement (LSCE), Institut Pierre Simon Laplace (CEA-CNRS-UVSQ UMR 8212), Gif-sur-Yvette, France

^b Department of Mathematics and Geosciences, University of Trieste, Italy

^c Department of Environmental Sciences, Informatics and Statistics, Ca' Foscari University of Venice, Italy

^d Department of Physics and Earth Sciences, University of Parma, Italy

^e Earth and Climate Cluster, Faculty of Earth and Life Sciences, Vrije Universiteit Amsterdam, Amsterdam, The Netherlands

^f Center for Climate and Resilience Research, University of Chile, Santiago, Chile

^g Laboratoire de Physique des Océans, UMR 6523, Université de Bretagne Occidentale, Brest, France

^h Centre for Ice and Climate, Niels Bohr Institute, University of Copenhagen, Copenhagen, Denmark

ARTICLE INFO

Article history:

Received 23 October 2014

Received in revised form

21 January 2015

Accepted 29 January 2015

Available online

Keywords:

Ice cores

Bipolar seesaw

Dansgaard Oeschger events

Water isotopes

ABSTRACT

Numerous ice core records are now available that cover the Last Glacial cycle both in Greenland and in Antarctica. Recent developments in coherent ice core chronologies now enable us to depict with a precision of a few centuries the relationship between climate records in Greenland and Antarctica over the millennial scale variability of the Last Glacial period. Stacks of Greenland and Antarctic water isotopic records nicely illustrate a seesaw pattern with the abrupt warming in Greenland being concomitant with the beginning of the cooling in Antarctica at the Antarctic Isotopic Maximum (AIM). In addition, from the precise estimate of chronological error bars and additional high resolution measurements performed on the EDC and TALDICE ice cores, we show that the seesaw pattern does not explain the regional variability in Antarctic records with clear two step structures occurring during the warming phase of AIM 8 and 12. Our Antarctic high resolution data also suggest possible teleconnections between changes in low latitude atmospheric circulation and Antarctic without any Greenland temperature fingerprint.

© 2015 Elsevier Ltd. All rights reserved.

1. Introduction

This introductory section summarizes the history of the identification of the bipolar seesaw pattern from Greenland and Antarctic ice cores (Section 1.1), and the ongoing debate on its causes and mechanisms, combining information from other natural archives, conceptual models, and a hierarchy of climate models (Section 1.2). From these open questions, it motivates the need for improved chronological constraints and high resolution, synchronized climate records documenting the spatial structure of changes in Greenland and Antarctica. The last Section 1.3 finally explains the structure of this manuscript.

1.1. Identification of the bipolar seesaw pattern from Greenland and Antarctic ice cores

Abrupt events punctuating climate variability of the Last Glacial period have been identified worldwide in highly resolved terrestrial, marine and ice core records (Voelker, 2002; Clement and Peterson, 2008). Since the 1960s, successive deep Greenland ice core records have provided continuous and extremely highly detailed records of climate variability, now encompassing the whole Last Glacial period, from 116 000 to 11 700 years ago recorded in GRIP (Dansgaard et al., 1993), GISP2 (Grootes et al., 1993), NorthGRIP (NorthGRIP Comm. Members, 2004) and NEEM ice cores (NEEM Comm. Members, 2013). During this time interval, 25 rapid events, called “Dansgaard-Oeschger events” (hereafter DO events), have been identified in numerous measurements performed along these Greenland ice cores (NorthGRIP

* Corresponding author. Tel.: +33 (0)169084672; fax: +33 (0)169087716.
E-mail address: amaelle.landais@lsce.ipsl.fr (A. Landais).

Community Members, 2004). Greenland abrupt temperature variations are qualitatively recorded at high resolution in water stable isotopes, while their magnitude is estimated using the thermal fractionation of gases inside the firn with an uncertainty of ~ 2 °C (Severinghaus and Brook, 1999; Kindler et al., 2014). Lasting a few centuries to a few millennia, DO events are characterized by the succession of a cold phase (Greenland Stadial, GS), an abrupt warming of 5–16 °C in a few years or decades, followed by a warm phase (Greenland Interstadial, GI) marked by a gradual cooling before a relatively abrupt cooling into the next GS, taking place within a few centuries. The widespread extent of DO events is reflected in parallel changes in the atmospheric composition (CH_4 concentration, as well as inflexions in the atmospheric $\delta^{18}\text{O}$ of O_2 , hereafter $\delta^{18}\text{O}_{\text{atm}}$) (Chappellaz et al., 1993, 2013; Landais et al., 2007). The strong abrupt temperature and CH_4 increases occur in phase, within 10 years (Severinghaus et al., 1998; Rosen et al., 2014). This abrupt variability in the atmospheric composition, being recorded in the air trapped in Greenland and Antarctic ice cores, has provided a critical tool for the transfer of the accurate Greenland age scales based on annual layer counting towards Antarctic ice core chronologies (Blunier et al., 1998; Schüpbach et al., 2011).

Since the 1970s, East Antarctic ice cores have also depicted millennial climate variability during the Last Glacial period, albeit with limitations in temporal resolution emerging from lower accumulation rates, and less accurate chronologies when annual layer counting is not possible. In Antarctic water stable isotope records, this millennial variability is marked by Antarctic Isotopic Maxima (AIM), initially identified in the central East Antarctic plateau as symmetric gradual isotopic enrichment (warming) and depletion (cooling) trends. Using a first synchronization of the Greenland GRIP and GISP2 ice cores with the Antarctic Vostok ice core through the alignment of $\delta^{18}\text{O}_{\text{atm}}$, Bender et al. (1994a) evidenced a recurrent relationship between Greenland and Antarctic water stable isotope millennial events for the nine longest GS. This Greenland and Antarctica pattern was also shown in parallel by Jouzel et al. (1994). A refined synchronization of Greenland (GRIP, GISP2) and Antarctic (Byrd) ice core records was built by Blunier et al. (1998) and Blunier and Brook (2001) based on the alignment of CH_4 records over the last 90,000 years. 7 main Antarctic warm events were identified (called A events) as Antarctic counterparts of major Greenland DO events. During each of these 7 events, Antarctic temperatures increased gradually during GS, and the end of Antarctic warming coincided with the onset of rapid warming in Greenland.

Using higher resolution data as well as an improved synchronization, it has been further evidenced that each DO event has an Antarctic Isotopic Maximum counterpart (EPICA Comm Members, 2006; Jouzel et al., 2007), except for the first DO event of the Last Glacial period identified in the NorthGRIP ice core, DO25 (Capron et al., 2012). The same bipolar characteristic was also identified at the sub-millennial scale, during GS precursors of DO, or rebound events at the end of GS, lasting only a few centuries (Capron et al., 2010a), albeit with the restrictions associated with the accuracy of the chronology, a few hundred years at best.

While there is growing evidence for the recurrence of abrupt climate change with similar characteristics during earlier glacial periods from high resolution Antarctic, terrestrial and deep sea records (e.g. McManus et al., 1999; Loulergue et al., 2007; Martrat et al., 2007; Barker et al., 2011; Lambert et al., 2012), we will focus here on the Last Glacial period for which the bipolar structure of events can be accurately characterized from high resolution and well dated records at both poles.

1.2. Causes and mechanisms of the bipolar seesaw

In parallel to ice core records highlighting millennial scale variability during the Last Glacial period, deep-sea sediments from the North Atlantic have revealed the recurrence of iceberg rafted debris in marine cores during GS, associated with iceberg discharges from glacial ice sheets, changes in sea ice extent, surface temperature and salinity, and reorganizations of the thermohaline circulation (e.g. Heinrich, 1988; Bond et al., 1992; Broecker et al., 1992; Grousset et al., 1993; McManus et al., 1998; Labeyrie et al., 1999; Elliott et al., 2002). Six major iceberg discharge episodes were identified as Heinrich events, corresponding to collapses of the Laurentide and/or European ice sheets (see review by Hemming, 2004). A Heinrich stadial was therefore defined as a Greenland cold phase during which a Heinrich event occurred (Barker et al., 2009; Sanchez-Goñi and Harrison, 2010). This feature led to the hypothesis that cold phases during Heinrich events (and, implicitly, all GS) were caused by changes in large scale Atlantic ocean circulation, driven by massive inflows of freshwater linked with glacial ice sheet collapses (e.g. Broecker, 1991; Paillard and Labeyrie, 1994; Ganopolski and Rahmstorf, 2001).

During the last decade, glacial abrupt events have been investigated using coupled ocean-atmosphere models of varying complexity (e.g. Stouffer et al., 2006; Kageyama et al., 2013). Several aspects of the observed patterns can be captured through the response of the Earth system to imposed freshwater perturbations in the North Atlantic (Ganopolski et al., 2001; Liu et al., 2009; Kageyama et al., 2010; Roche et al., 2010), mimicking Heinrich events. Depending on the background state of the climate (glacial or interglacial, orbital context ...), of the simulated Atlantic Meridional Oceanic Circulation (AMOC), and the magnitude of the freshwater forcing, these models can produce a complete shutdown of the AMOC (Heinrich-like state) or a reduction of the strength of the AMOC (GS-like state) (e.g. Menviel et al., 2014). In all models, the injection of freshwater robustly produces a significant cooling of the North Atlantic region. The amplitude of the associated temperature change is probably affected by the simulated change in sea-ice extent and feedbacks between sea-ice and temperature that vary in the different models (Kageyama et al., 2013). These hosing experiments also produce an inter-hemispheric seesaw temperature pattern and impacts on the position of the intertropical convergence zone, hereafter ITCZ (e.g. Dahl et al., 2005; Broccoli et al., 2006; Krebs and Timmermann, 2007; Swingedouw et al., 2009) through changes in meridional heat transport. In response to freshwater forcing, climate models simulate a decrease of the NADW (North Atlantic Deep Water) export and a possible increase of the AABW (Antarctic Bottom Water) export in the Southern Ocean (Rind et al., 2001). The alternation between NADW and AABW formation is supported by paleoceanographic deep circulation tracers (e.g. review by Adkins, 2013), as well as by changes in ^{14}C of CO_2 measurements (Broecker, 1998; Anderson et al., 2009). The different models confirm the robustness of the bipolar seesaw signature of the climate response to AMOC weakening with the South Atlantic systematically warming in response to a freshwater discharge applied in the North Atlantic. There are still regional differences in the simulated Southern Ocean response (Clement and Peterson, 2008; Kageyama et al., 2010; Timmermann et al., 2010). Some models simulate a quasi-uniform warming (e.g. Otto-Bliessner and Brady, 2010) while others show contrasted patterns with a West Pacific cooling associated with the Southern Indian Ocean sector warming.

Conceptual models, paleoceanographic data and climate models of varying complexity all converge to show that DO events are associated with changes in AMOC. However, a number of physical

mechanisms allowing quasi-periodic transitions between different modes of operation of the AMOC have been proposed. Among them one must distinguish between those where abrupt millennial climate shifts result from changes in external forcing (e.g. freshwater cycle, solar cycle) from those where either internal instabilities of the large-scale ocean circulation or nonlinear sea ice – ocean – ice sheet interactions play a fundamental role. Recent modeling studies suggest that the relatively weak Atlantic northward heat transport that prevails under cold background conditions is the key to the existence of such instabilities (Arzel et al., 2010; Colin de Verdière and te Raa, 2010; Arzel et al., 2012). In those studies, ice-sheet ocean interactions, atmospheric noise or time-varying external forcing are not essential to the emergence of millennial climate shifts. Glaciological studies have stressed that calving due to internal Laurentide ice sheet instabilities can deliver massive meltwater fluxes albeit with large uncertainties on the exact timing, magnitude and rate of delivery (MacAyeal et al., 1993; Marshall and Clark, 1997). Such calving events and associated meltwater – induced climate variability can be reproduced in climate models of reduced complexity (Ganopolski, 2003; Ganopolski et al., 2010). Whether the iceberg discharge is a cause or a consequence of changes in AMOC is however an open question. Indeed, a reduced AMOC can also trigger subsurface warming and instabilities of ice streams (Shaffer et al., 2004; Alvarez-Solas et al., 2011, 2013; Marcott et al., 2011). Changes in atmospheric circulation in relationship with changes in sea ice extent and/or changes in ice sheet topography may also cause abrupt glacial climate shifts (Wunsch, 2006; Li et al., 2010; Zhang et al., 2014).

The initial trigger of instabilities may not lie within the North Atlantic, which could just act as an amplifier (Cane and Clement, 1999). Several authors have explored the possible role of Antarctic freshwater fluxes on AMOC instabilities. For instance, Weaver et al. (2003) suggested an Antarctic origin of meltwater pulse 1A. This 14–18 m global mean sea level rise occurred during the abrupt Bølling-Allerød warming (Deschamps et al., 2012). While there is evidence for West Antarctic ice retreat coeval with MWP1A (Kilfeather et al., 2011; Smith et al., 2011), the magnitude of the Antarctic contribution remains disputed (Clark et al., 2009; Bentley et al., 2010; Mackintosh et al., 2011; Golledge et al., 2014), as glaciological studies indicate possible large contributions from North America (Carlson and Winsor, 2012; Gregoire et al., 2012). Idealized Southern Ocean hosing simulations do not produce large Greenland warming (Seidov et al., 2005; Stouffer et al., 2007; Swingedouw et al., 2008) and are thus suggesting that Antarctica cannot be the driver of DO events. Intrinsic instabilities of the Southern Ocean stratification have also been found in climate models of intermediate complexity (Meissner et al., 2006). These instabilities generate abrupt multi-millennial oscillations whose mechanism is essentially captured by the Welander (1982) two-box model. Corresponding changes in surface air temperature reach a few degrees in the Southern Ocean with little impact in the Northern Hemisphere.

Finally discriminating the respective role of changes in AMOC with respect to changes in sea ice extent and atmospheric circulation and identifying the trigger for the millennial variability calls for very high resolution paleoclimate records, an accurate identification of the north-south timing of changes, and the characterization of regional patterns of changes.

1.3. Structure of this manuscript

In this manuscript, we focus on the last 60 000 years where our bipolar chronological framework is most accurate, thanks to layer counting for Greenland ice cores and numerous age markers, using the latest available common chronology for Greenland and

Antarctic ice core, AICC2012 (Bazin et al., 2013; Veres et al., 2013). The accuracy and limitations of the chronology are specifically addressed in Section 2. The temporal relationships between Antarctic and Greenland temperature over the Last Glacial cycle will be discussed in Section 3 using the AICC2012 chronology. This will include new highly resolved measurements of water stable isotopes from two East Antarctic ice cores (EDC and TALDICE). The comprehensive picture of the see-saw sequence, including regional variability among East Antarctic sites is discussed in Section 4. Finally, Section 5 addresses perspectives to progress in the understanding of mechanisms driving Greenland-Antarctic abrupt climate variability through the use of multiple tracers of climate at lower latitudes, as well as insights expected from earlier glacial periods.

2. The bipolar seesaw using the AICC chronology and age scale uncertainties

2.1. Methods for Greenland and Antarctic age scale synchronization and AICC2012

For a discussion of bipolar seesaw, we concentrate here on the relative uncertainty between Antarctic and Greenland chronologies.

A critical limitation for the description of the sequence of Greenland versus Antarctic climate change is linked to the difficulty of synchronizing different ice cores at high temporal precision. Through time, a collection of absolute and relative ice core dating constraints has been accumulated. For instance, the identification of the Laschamp geomagnetic excursion in the ^{10}Be concentration in different ice cores allows to transfer the absolute age of the excursion, from radiometric dating methods applied on lavas (e.g. Guillou et al., 2004; Singer et al., 2009) to ice core records (Raisbeck et al., 2007). Several parameters provide tools for the synchronization of ice core records. They arise from the global variability of well mixed atmospheric gases and high resolution measurements of CH_4 and $\delta^{18}\text{O}$ of O_2 in the gas phase of ice cores (e.g. Capron et al., 2010); or from the occurrence of volcanic events, whose fingerprints can be identified from chemical (major ion concentrations) or physical (electrical conductivity, particles) measurements performed on the ice phase (e.g. Parrenin et al., 2012a).

A specific uncertainty arises from the need to build two different timescales for each ice core, one for the ice phase and one for the gas phase. Age differences between ice and gas at a given depth arise from the firnification processes, when snow is consolidating to ice and the air is trapped inside, at the lock-in depth (LID), about 100 m under the ice-sheet surface. Because firnification processes (and therefore the LID) are affected by changes in temperature, accumulation rate, and possibly by the snow impurity content (Hörhold et al., 2012), the gas age – ice age difference varies through time and space with variations of several thousands years for ice cores of the East Antarctic plateau (EPICA Dome C, Vostok).

During the past 60,000 years, the Greenland ice core GICC05 chronology is based on multi-parameter layer counting and provides a reference ice age scale. The absolute uncertainty of the GICC05 chronology used as a reference for the last 60 ka for AICC2012 has no importance for the bipolar seesaw pattern which is investigated here. On opposite, the gas chronology calculated for NorthGRIP has an impact on the seesaw pattern because of gas stratigraphic links in between ice cores. It therefore needs to be precisely constrained. Due to relatively high accumulation rates, the gas age – ice age difference, Δage , remains small in Greenland (<1000 years) and is very well simulated by firn models. This is verified using markers of abrupt local warming in the gas phase, through abrupt changes in inert gas isotopic composition caused by

firm air thermal fractionation (e.g. Kindler et al., 2014). The depth difference, Δ_{depth} , between the same event (an abrupt warming), recorded in the gas phase (a peak of $\delta^{15}\text{N}$) and in the ice phase (an abrupt increase in ice $\delta^{18}\text{O}$) enables to constraint the gas chronology vs. the ice chronology in Greenland with minimal uncertainties (Rasmussen et al., 2013).

The transfer of this Greenland gas chronology towards the Antarctic gas chronology relies on the global signals provided by changes in atmospheric composition (in the gas phase). The accuracy of this transfer is only limited by the resolution of the records and the smoothing caused by firn diffusion (Köhler et al., 2011).

A major source of uncertainty for the investigation of the precise temporal sequence between changes in Greenland and Antarctic water stable isotope records (both in the ice phase) arises from the construction of the Antarctic ice age scale from the gas age scale synchronized with that of Greenland. It mostly depends on the ability to accurately estimate the temporal evolution of the LID in Antarctica. Several studies have therefore taken advantage of Antarctic ice cores in the least dry areas (West Antarctica for Byrd or Siple Dome, coastal East Antarctica for Law Dome), where the gas age – ice age difference, Δ_{age} , is smallest (several hundreds of years) which limits the associated uncertainty (e.g. Blunier et al., 1998; Pedro et al., 2012). Uncertainties are largest for the dry central East Antarctic sites, where, under glacial conditions, Δ_{age} differences can reach several thousand years.

The estimates of past LID based on firnification models are probably associated with an uncertainty of about 20% (Landais et al., 2006; Parrenin et al., 2012b). However, the combination of stratigraphic constraints in both the gas and in the ice phases in different ice cores narrows LID estimates. Moreover, constraints on past LID can also be established using air $\delta^{15}\text{N}$ in Antarctic ice cores (Parrenin et al., 2012b). $\delta^{15}\text{N}$ is mainly affected by gravitational fractionation in the air circulating in the diffusive zone of the unconsolidated snow. It is therefore directly proportional to the depth of the diffusive column, and therefore to the changes in LID.

While the first Greenland–Antarctic chronologies were manually established from the interpolation of a few age markers, site by site, the AICC2012 timescale has been produced as a community effort for the collection of dating constraints and their integration using a common mathematical framework applied to several deep ice cores. Using a Bayesian tool dedicated to multi-ice cores dating, Lemieux-Dudon (2010), Bazin et al. (2013) and Veres et al. (2013) have built a coherent chronology integrating 5 ice cores from Greenland (NorthGRIP) and Antarctica (EPICA Dome C – EDC –, EPICA Dronning Maud Land – EDML –, TALDICE, Vostok, Fig. 1).

The AICC2012 effort has gathered an unprecedented high number of stratigraphic tie-points between the Greenland NorthGRIP and the 4 Antarctic ice cores and between Antarctic ice cores. The AICC2012 synchronization uncertainty (Fig. 2) mostly arises from (i) the density of gas markers (mainly methane) and their associated uncertainties (Loulergue, 2007; Loulergue et al., 2007; Lemieux-Dudon et al., 2010; Schilt et al., 2010; Capron et al., 2010b; Buiron et al., 2011; Schüpbach et al., 2011; Bazin et al., 2013); (ii) the density of ice markers (volcanic eruption and ^{10}Be peak around the Laschamps event) and their associated uncertainties (Udisti et al., 2004; Loulergue et al., 2007; Ruth et al., 2007; Severi et al., 2007, 2012; Parrenin et al., 2012a; Bazin et al., 2013; Svensson et al., 2013); (iii) the determination of the LID in the different ice cores and their associated uncertainties. Fig. 3 displays the different age markers used in AICC2012 and the associated uncertainties over the last 60 ka (Bazin et al., 2013; Veres et al., 2013). It illustrates how the final relative uncertainties of each Antarctic ice core chronology (relative to NorthGRIP) are strongly linked to these gas and ice markers.



Fig. 1. Location of the Antarctic cores included in the AICC2012 chronology. The red points highlight the sites that are considered in this study.

Between 26 and 17 ka, in the absence of any tie points, chronology uncertainties strongly increase (Fig. 2). Uncertainties of only a few centuries occur when both gas and ice tie points are present. This is the case around the Laschamp event at ~ 41 ka which concentrates methane tie points for each DO event, numerous volcanic tie points between the Antarctic ice cores, and the ^{10}Be fingerprint of the Laschamp events in Greenland and Antarctic ice cores. Note that we have excluded Vostok from the following discussion because of too weak dating constraints linked to the low resolution of the initial records.

2.2. Uncertainty associated with AICC2012

Here, three issues are discussed with respect to the north-south sequence of events: first, we investigate the uncertainty associated with the estimation of LID at EDC and EDML; second, we revise the estimation of the NorthGRIP LID between DO events which was likely overestimated in AICC2012; third, we discuss the calculation of the AICC2012 uncertainty.

In the construction of AICC2012, the LID background scenarios were driven by the $\delta^{15}\text{N}$ profile measured in ice cores. Parrenin et al. (2012b) indeed demonstrated that for EDC, the LID was better estimated from $\delta^{15}\text{N}$ than when using a firnification model. Still, $\delta^{15}\text{N}$ will not be linearly related to the LID if there are changes in firn convective zone. As a consequence a large variance was associated with the background LID scenario in the building of AICC2012 with DATICE. However, the link between the value of the variance of the background scenario and the final DATICE uncertainty is not straightforward and the chronological uncertainty resulting from the LID uncertainty in Antarctic ice cores may have been overestimated in AICC2012.

The uncertainty associated with the background LID is addressed here by sensitivity tests with DATICE (Fig. 3). Simulations have been performed with different background scenarios for EDC, TALDICE and EDML LID for two extreme cases: either from $\delta^{15}\text{N}$ measurements (which leads to the lowest possible value of the LID) or from the firnification model (Goujon et al., 2003, leading to an upper estimate for LID). Using a LID deduced from the firnification model leads to systematically larger glacial Antarctic LID than when using the $\delta^{15}\text{N}$ measurements. Antarctic chronologies are therefore systematically older than AICC2012 by up to 500 years around the LGM (red lines, Fig. 3). This chronological change is minor. Indeed, the multiplicity of gas and ice stratigraphic tie-points used in

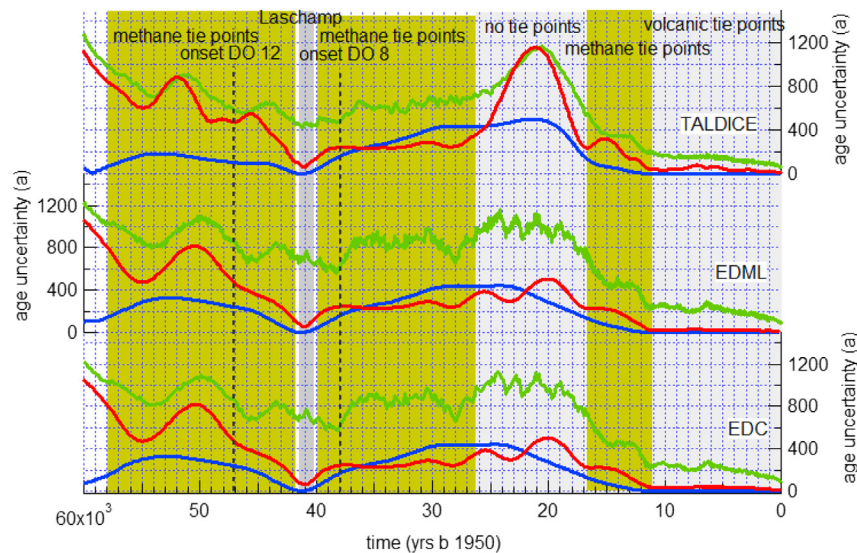


Fig. 2. Illustration of the sources of uncertainty in the AICC2012 chronology: in green the total uncertainty of AICC2012; in blue, the chronology difference induced by different estimates of the background LID (either from firnification model or from $\delta^{15}\text{N}$ data); in red, the ice uncertainty calculated by DATICE. The EDC and EDML AICC2012 uncertainties are similar because of the numerous ice tie points between them (see details in SOM of Bazin et al., 2013). Note that this chronology was built with an artificially small uncertainty on the NorthGRIP GICC05 chronology (<20 years over the last 60 ka) so that the displayed uncertainty actually reflects the relative uncertainties of each Antarctic ice core relative to NorthGRIP.

DATICE compensates for the large uncertainty in the background LID scenario. The phasing between Antarctica and Greenland over DO/AIM events is not significantly affected. For DO/AIM 8 (Fig. 3b), the Greenland vs Antarctica phasing is exactly the same for the two different background scenarios of LID because of the proximity of the Laschamp event providing ice stratigraphic tie-points. For DO/AIM 12 (Fig. 3c), the Antarctic records are slightly older by a few centuries, but this does not affect the Greenland vs Antarctica seesaw pattern.

Despite strong and robust constraints at the onset of each DO events from $\delta^{15}\text{N}$ measurements (Huber et al., 2006; Kindler et al., 2014), the NorthGRIP LID was not properly estimated between DO events. This is due to the combined effects of two strong constraints imposed on the NorthGRIP chronology in AICC2012 as explained in the following. First, for the onset of each DO event, Δ depth constraints were provided as inputs to DATICE based on the synchronicity of the two temperature-sensitive records ($\delta^{18}\text{O}$ increase in ice and $\delta^{15}\text{N}$ increase in gas). Then, by construction, AICC2012 was driven by the GICC05 Greenland chronology and with an imposed thinning function for NorthGRIP (NorthGRIP members, 2004). The combination of imposed Δ depth and thinning led DATICE to overestimate NorthGRIP LID by up to 10–20 m, especially around DO 12, compared to the estimate based on $\delta^{15}\text{N}$ and firn modeling (Kindler et al., 2014). Bazin et al. (2014) solved this problem by allowing DATICE to modify the NorthGRIP thinning scenario, thus leading to a smaller NorthGRIP LID. The revised Antarctic chronologies produced this way are independent of GICC05 and show small differences with AICC2012 (<400 years). They do not affect significantly the Antarctica vs. Greenland relationship, especially over DO/AIM 12 and DO/AIM 8, this last sequence being particularly well constrained by tie-points around the Laschamp event (Fig. 3b and c).

Antarctic chronologies are mainly based on gas tie points between Greenland and Antarctica, so that the ice chronology is deduced from the gas chronology and thus must incorporate uncertainties associated with the LID estimates. This is however not always the case in DATICE when many ice stratigraphic tie points are present, especially between EDML and EDC (76 ice stratigraphic tie-points over the period 30 to 60 ka). Because a correct

reformulation of the error calculation requires significant developments, AICC2012 reported the gas chronological uncertainty, which considers the uncertainty associated with LID, in addition to the uncertainties associated with the ice chronology in DATICE (i.e. stratigraphic and absolute tie points and variance associated with thinning and accumulation rate background scenarios). This formulation is correct when only gas tie points are present, but it is an overestimation of the true uncertainty when mainly ice tie-points are present (Holocene or around the Laschamp event). In this case, the uncertainty attached to the ice chronology should be used for the comparison of water stable isotope records.

Fig. 2 compares two estimates of the ice chronological uncertainty: DATICE uncertainty for the ice chronology (red) and AICC2012 official uncertainty mainly obtained from DATICE uncertainty on the gas chronology (green). As explained above, these uncertainties should be taken as an Antarctica–Greenland synchronization uncertainty. Around the Laschamp event, the difference between the two types of uncertainties is ~400 years at EDML and EDC. We argue that it is overestimated by DATICE in AICC2012. Indeed, for this period, the maximum difference between chronologies obtained with extremely different LID background scenarios is less than 200 years (red and blue lines, Figs. 1, and 2). The relative ice chronological uncertainty between Antarctic (EDC, EDML, TALDICE) and NorthGRIP at the time of DO-AIM 8, very close to the Laschamp event, should therefore be less than 400 years.

For DO 12, the situation is different since there is no ice tie-point common to Greenland and Antarctica (Bazin et al., 2013). There is therefore no reason to challenge the AICC2012 uncertainty of 600–700 years given for the relative chronology between Antarctic and Greenland ice as a correct upper boundary.

3. Water stable isotope records of bipolar seesaw

3.1. Stack Greenland and Antarctic records on AICC2012

In order to extract the common East Antarctic signal, we have combined the water isotopic records for the 4 Antarctic ice cores synchronized on AICC2012 to obtain an East Antarctic isotopic

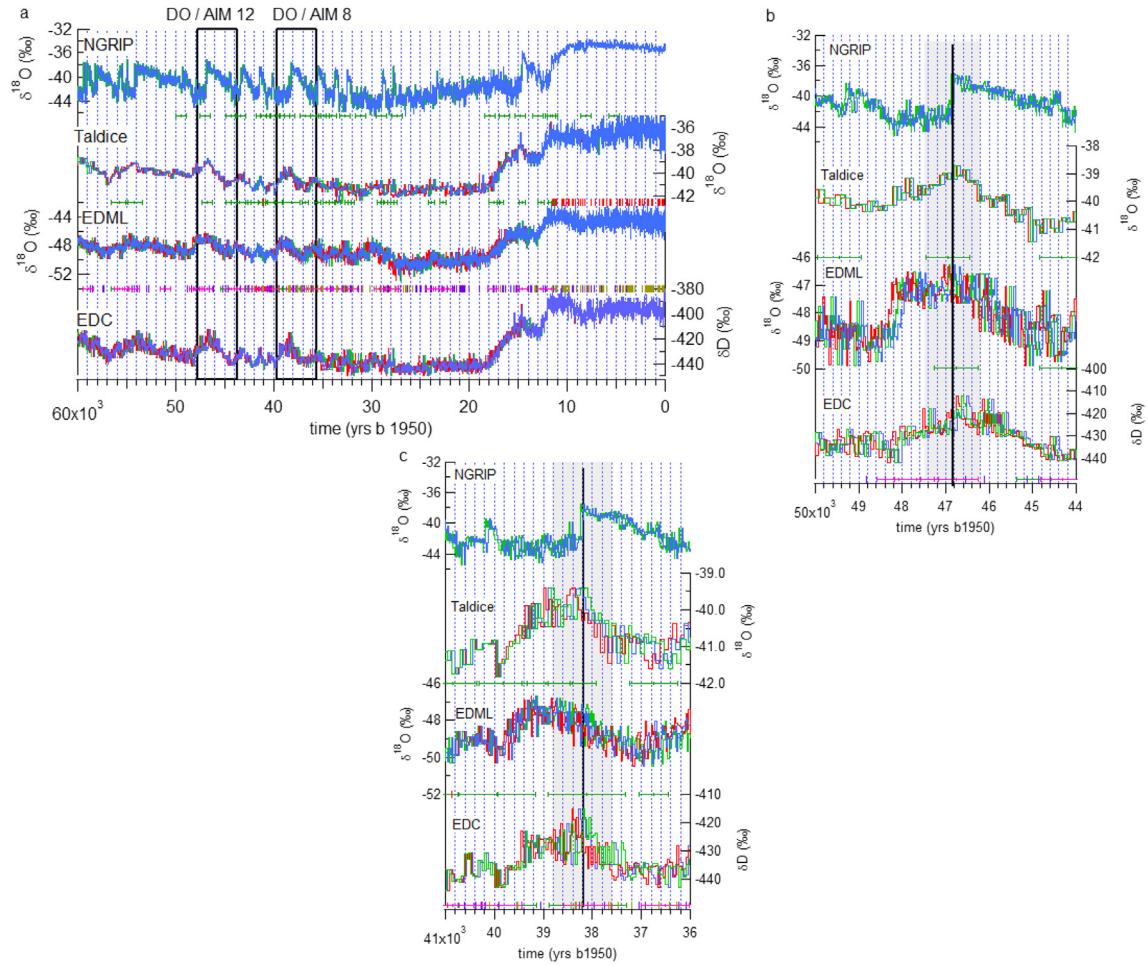


Fig. 3. a) NorthGRIP, Taldice, EDML and EDC $\delta^{18}\text{O}$ profiles (55 cm resolution) on AICC2012 (blue) with the identification of the large DO events 8 and 12 (black rectangles). Horizontal markers indicate the position and uncertainties of ice and gas stratigraphic links (green – ice stratigraphic links between EDC and TALDICE; blue – ice stratigraphic links between EDC and EDML; purple – gas stratigraphic links between EDC and EDML). b) Same as (a) but for a zoom on DO 12. c) Same as (a) but for a zoom on DO 8. The red line depicts the results of DATICE calculations when using LID calculations based on firnification model rather than $\delta^{15}\text{N}$ data (as in AICC2012). The green line is the output of DATICE without the strong GICC05 constraints (here we show the run with correlation of NorthGRIP markers of age difference from Bazin et al. (2014) which shows the largest difference to AICC2012). The black lines on Fig. 3b and c shows the onset of DO events in Greenland and the gray rectangles the AICC2012 uncertainty of EDML and EDC chronology for this onset.

stack. From the available resolution of individual records, the East Antarctic stack has been produced with a 100 year resolution. For Greenland, we have used the available synchronization of the Greenland ice cores (GRIP, GISP2 and NorthGRIP) performed during the construction of the GICC05 timescale (Svensson et al., 2008 and references herein) to obtain a Greenland isotopic stack on the AICC2012 timescale. These two stacks clearly show the classical

bipolar seesaw pattern (Fig. 4), with Antarctic warming during GS, particularly visible for long stadials (e.g. DO 21, 12, 8). During the shortest stadials, the common Antarctic signal is equivocal, due to the noise caused by small chronological shifts, noise and regional differences in water stable isotope patterns (see next section).

The global picture of the bipolar seesaw highlighted in Fig. 4 is in general agreement with the simple modeling of Stocker and

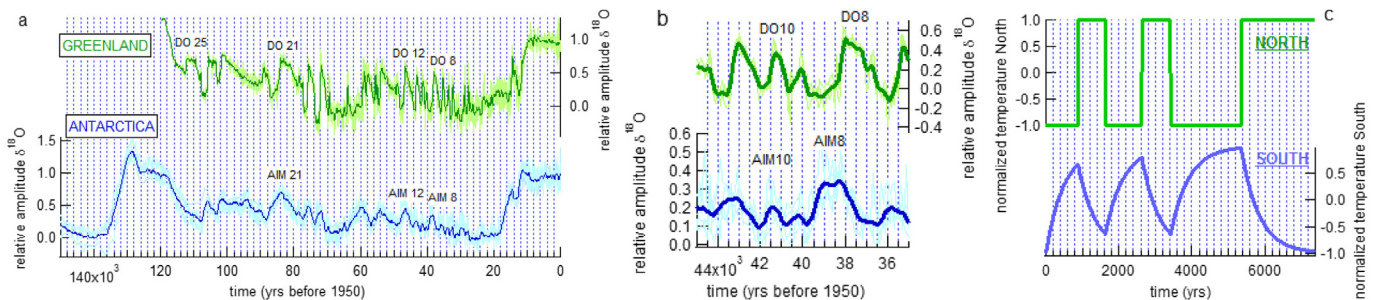


Fig. 4. a) Stack of East Antarctic (Vostok, EDML, EDC and Taldice) $\delta^{18}\text{O}$, and Greenland (GRIP, GISP2, NorthGRIP) $\delta^{18}\text{O}$ on AICC2012/GICC05 synchronized chronologies, expressed in relative amplitude centered onto the present-day value. The average stack value is depicted with the bold colored lines, while the individual ice core records are shown in light color. b and c) Comparison between the data around DO 8–12 and the results of the thermodynamical model of Stocker and Johnsen (2003).

Johnsen (2003) for the slow thermal response of Antarctic temperature to Greenland abrupt warmings and coolings through a heat reservoir in the southern ocean.

3.2. Regional differences in Greenland and Antarctica

Spatial gradients have already been evidenced in Greenland based on temperature (derived from $\delta^{15}\text{N}$), accumulation, and $\delta^{18}\text{O}$ records (e.g. Guillevic et al., 2013; Buizert et al., 2014). Using NEEM, NorthGRIP and Summit ice cores during the last deglaciation and over DO event 8, they have shown that, while the magnitude of $\delta^{18}\text{O}$ changes is largest at NEEM, the magnitude of abrupt warming is largest in central Greenland (Summit). These studies have confirmed the validity of $\delta^{18}\text{O}$ as a qualitative temperature proxy, but revealed that, in Greenland, it is not a reliable indicator of the amplitude of abrupt warming. The pattern of temperature change associated with abrupt warming can be potentially explained with the impacts of changes in Nordic sea ice cover (Li et al., 2005) and the impacts of changes in AMOC on Greenland climate (Buizert et al., 2014).

In Antarctica, no independent paleothermometry method has yet been applied for AIM events, restricting the investigation of the patterns and rates of changes to $\delta^{18}\text{O}$ only. Existing simulations performed with isotope enabled atmospheric general circulation models stress the reliability of the isotope–temperature relationship under glacial boundary conditions (e.g. Werner et al., 2001; Jouzel et al., 2013). We will therefore use isotopic rates of changes through time to identify patterns of rates of warming during AIM events.

The new AICC2012 timescale allows investigating regional patterns in Antarctica. Stenni et al. (2010) already stressed a square shape of AIM in the Atlantic sector (EDML), which contrasts with the triangular (symmetric) shape of AIM events in the Indo-Pacific sector (EDC, Vostok, TALDICE, Byrd, WAIS ...). During the warming phase of the largest AIM events of the last 50 ka, Buiron et al. (2012) estimated that the rate of warming (isotopic enrichment) was twice smaller at TALDICE and EDC than at EDML. This feature is confirmed using the AICC2012 timescale.

We now focus on EDML, TALDICE and EDC (Fig. 5) for which (i) high resolution water stable isotope records are available (respectively 20, 50 and 70 years for EDML, EDC and TALDICE around AIM 8, at ~38 ka), and (ii) age scale uncertainties are the smallest (Fig. 2). We do not discuss the Vostok ice core which has lower resolution and chronological accuracy. The maximum ice age uncertainty around AIM 8 and AIM 12 estimated through AICC2012 is respectively ± 600 years for TALDICE and ± 800 years for EDML and EDC. Because of this uncertainty, it is impossible to investigate regional differences during the small and short-lived D/O events of MIS 3.

A clear picture nevertheless emerges for AIM 8 (Fig. 5), where the sharp water stable isotope increase recorded at EDML ends 1200 ± 600 years earlier than the onset of abrupt Greenland warming and hence only 600 years after the preceding Greenland cooling. The first gradual isotopic enrichment recorded at EDC starts in phase with this EDML warming when Greenland is cooling. Because of the numerous ice stratigraphic links between EDML and EDC, their relative ice chronological uncertainty is only ± 200 years. This first rapid warming at EDC is followed by a gradual temperature increase along the 1200 years preceding Greenland abrupt warming when EDML $\delta^{18}\text{O}$ is on a plateau. Similar patterns are depicted at TALDICE albeit with lower temporal resolution. By contrast, the slow cooling phase following abrupt Greenland warming occurs in phase for all Antarctic ice cores, and in phase with the slow GIS cooling. The same characteristics are also observed during AIM 12: at EDML, a very fast warming ends about 1200 years prior to Greenland abrupt warming, followed by a long

lasting plateau; at EDC and TALDICE, the warming phase occurs in two steps (Fig. 5).

Exploring the uncertainties attached to the relative AICC2012 chronologies between EDML, EDC, TALDICE and NorthGRIP ice cores (Fig. 3) confirms the robustness of this sequence of events around AIM 8 and 12. Revised estimates of LID indeed produce older Antarctic ice ages and therefore a longer lag between the first Antarctic warming phase and the onset of Greenland interstadial.

3.3. New high resolution water stable isotope data

To further explore the identified inflexion points in TALDICE and EDC, we report here the additional information provided by new high resolution water stable isotope data for these two sites.

The initial EDC δD and $\delta^{18}\text{O}$ profile from EDC were obtained along 55 cm long ice “bag” samples (Jouzel et al., 2007; Stenni et al., 2010). While they document Holocene climate with a resolution of ~20 years (Pol et al., 2011), ice thinning and lower glacial accumulation rates result in a loss of temporal resolution for glacial climate variability (50 year resolution). Higher resolution records have therefore been obtained from more than 8000 new $\delta^{18}\text{O}$ measurements performed using 5 sections of 11 cm within each bag sample. These new mass spectrometry measurements have an accuracy of 0.07‰ using a classical method of water/ CO_2 equilibration at the Center for Ice and Climate of the University of Copenhagen.

The high resolution data confirm all the details of the low resolution signals available from bag measurements (Jouzel et al., 2007; Stenni et al., 2010). They reveal centennial variability within AIM which was not visible in bag measurements and preferentially occurs during the warm and warming phases of AIM (Fig. 6, red rectangles). These short-lived, sharp events reach a magnitude $>2\%$ (2.6 °C using the spatial isotope–temperature relationship) in about 20–30 years. AIM 8 and 12 are characterized by a multi peak structure around the maximum $\delta^{18}\text{O}$ level of the AIM and one peak during the warming phase, at the inflexion point between the two warming phases at EDC (vertical bar b on Fig. 6b and c). These peaks are also visible through excursions in the calculated 200 years running variance (Fig. 6b and c). In addition, two events occur during the peak and cooling phase of AIM 14, potentially synchronous with sub-event 14-b recorded in NorthGRIP (Rasmussen et al., 2013). Finally, the two events occurring at peak warmth of AIM 16 coincide within chronological uncertainty with the large centennial variability in Greenland (events DO 16.1 and 16.2 as defined by Rasmussen et al., 2013). Similar events may have occurred during AIM 0 (early Holocene optimum) and Last Interglacial early optimum, as recorded in “fine cut” samples δD (Pol et al., 2011, 2014).

We now investigate the patterns of TALDICE $\delta^{18}\text{O}$ variability using new measurements. The initial TALDICE $\delta^{18}\text{O}$ profile was obtained at 1 m resolution (Stenni et al., 2011; Buiron et al., 2012), leading to 100 years resolution for the Last Glacial period. New high resolution $\delta^{18}\text{O}$ measurements spanning AIM 8 and AIM 12 were therefore performed at 10 cm resolution at Parma and Trieste Universities using the classical method of water/ CO_2 equilibration. Again, the high resolution $\delta^{18}\text{O}$ measurements confirm the details of the initial record (Fig. 6) and clearly depict centennial variability. Both at EDC and TALDICE, the data depict an optimum coinciding with the end of the EDML warming phase. This first optimum is more strongly marked at TALDICE, followed by a “cold-reversal-type” drop, labeled “L” on Fig. 6 and associated with a decrease of the 200 years running variance (Fig. 6b and c). We do not detect the same sharp events as recorded in EDC, questioning the spatial structure of such sharp, short-lived events. Backward trajectory analysis (Scarchilli et al., 2011) suggests that TALDICE is influenced

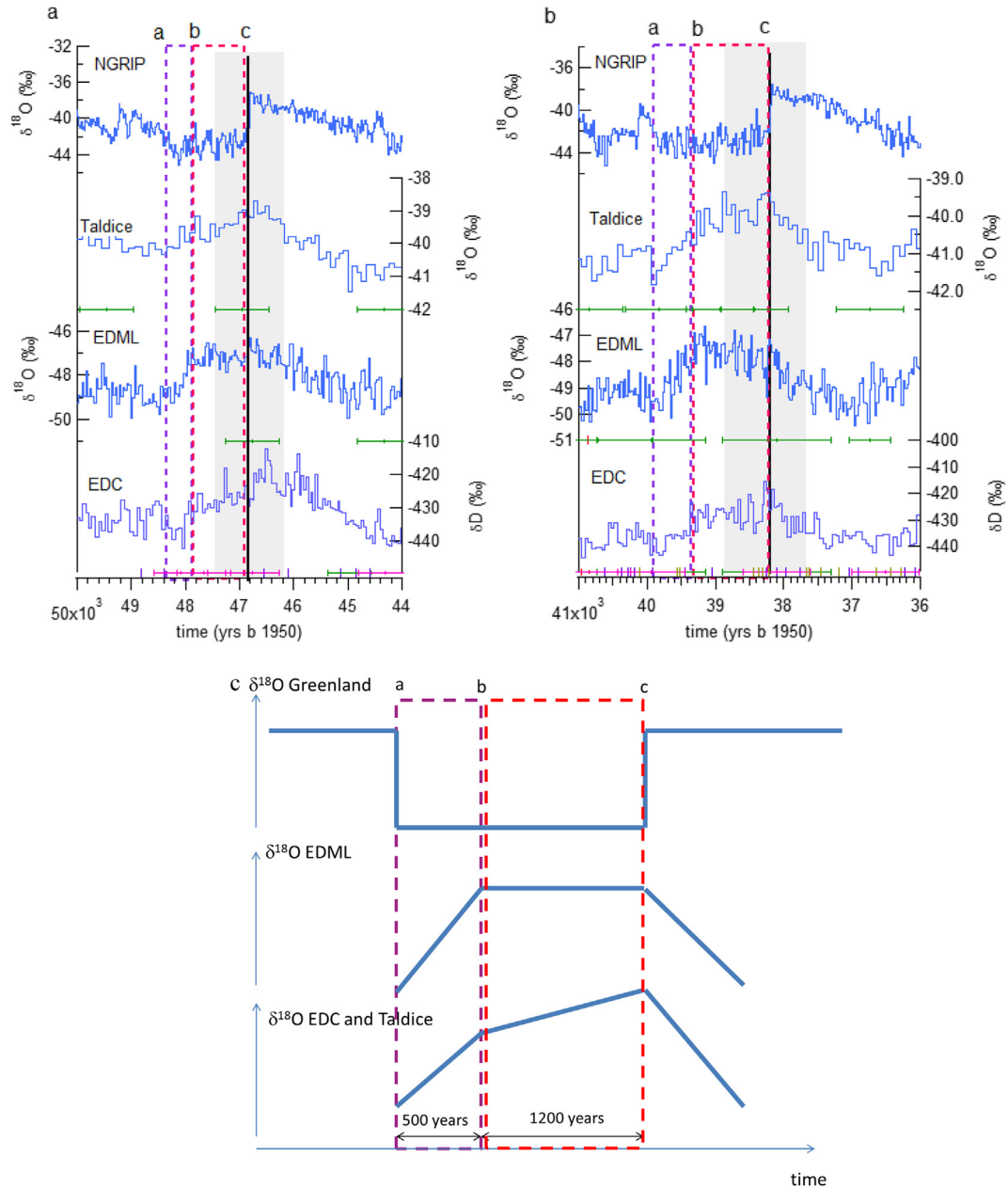


Fig. 5. Focus on DO-AIM 12 (a) and 8 (b). From top to bottom: $\delta^{18}\text{O}$ records from NorthGRIP, Taldice, EDML and EDC, on the AICC2012 chronology. Horizontal error bars in panels (a) and (b) stress the position of ice and gas stratigraphic links between EDC, TALDICE and EDML. Panel (c) provides a schematic representation of the structure of $\delta^{18}\text{O}$ changes identified during both events. Shaded rectangles highlight the chronological uncertainties for the AIM 12 and 8 in panels a and b. The violet and red rectangles highlight the separation in two phases for the warming of the AIM in each of the 3 panels and the letters a, b and c mark the separation between each phases as used in the following figures.

by moisture originating mainly from the Indian and secondarily from the Pacific sectors of the Southern Ocean, while EDC is mainly influenced by the Indian Ocean. Differences between EDC and TALDICE could thus be linked to different transport paths compared to present day but also to possible differences in their sensitivity to sea-ice variability, mainly due to their different distance to the coast.

We conclude that high resolution data from EDC and TALDICE confirm the three phase structure of AIM8 and 12, with TALDICE showing a marked optimum (followed by a minimum) at the end of the EDML warming phase (vertical bar b on Fig. 6b and c) corresponding to the inflexion between the first and second EDC and EDML warming phases. At EDC, the data depict short-lived, sharp events with a large isotopic anomaly, during the warm phases of

AIM events, when Greenland abruptly warms (vertical bar c on Fig. 6b and c). Similar events are seen at the inflexion between the first and second EDC and EDML warming phases (vertical bar b on Fig. 6b and c).

4. Discussion

The structure of Antarctic $\delta^{18}\text{O}$ records depicts a variability which does not follow a simple bipolar seesaw scheme, both in the sharp events depicted in high resolution data from EDC and TALDICE, and in the two phase structure observed during major Antarctic warmings (AIM 8 and AIM 12 warming phases). These patterns can therefore not be explained by a simple seesaw mechanism implying a slow response of Antarctic temperature to

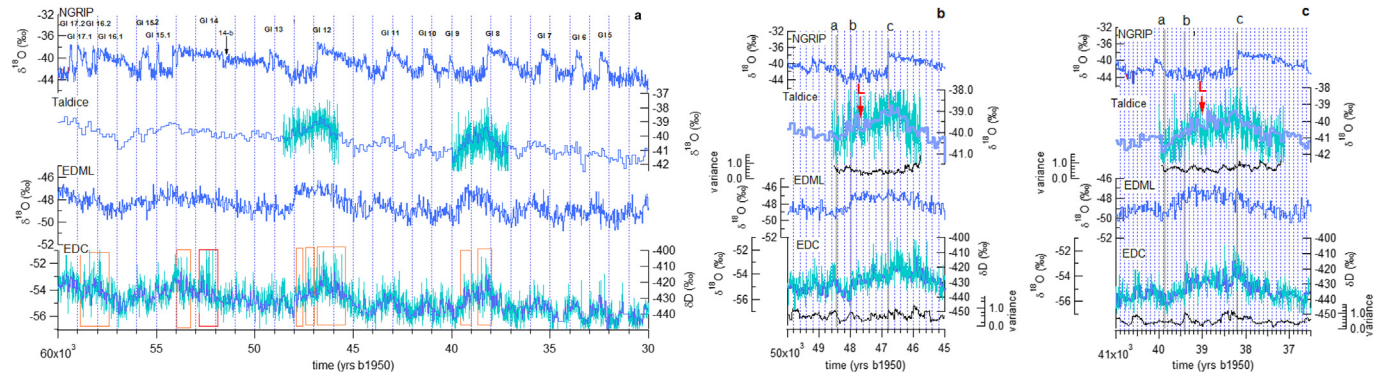


Fig. 6. a) new high resolution water stable isotope measurements from TALDICE and EDC (light blue), superimposed on existing low resolution data (blue) on AICC2012. b) Same as (a) but for a zoom on AIM 12. The 200 year running variance for the Taldice and EDC high resolution data are added. The vertical bars a, b and c respectively indicate the beginning of the GS/AIM, the inflexion point at the end of the EDML $\delta^{18}\text{O}$ increase and EDC main $\delta^{18}\text{O}$ increase and the abrupt warming in Greenland. c) Same as (b) but for AIM 8.

abrupt North Atlantic climate shifts, modulated by the thermal inertia of the southern ocean. Several hypotheses can be formulated. One option is that this Antarctic variability reflects abrupt changes in atmospheric circulation and/or moisture origin, probably linked to sea ice variability. A second option is that Greenland climate (temperature, accumulation and $\delta^{18}\text{O}$) does not reflect changes in North Atlantic ocean circulation. To explore the first option, we compare the Antarctic $\delta^{18}\text{O}$ records with aerosol and deuterium excess data (Section 4.1). To explore the second option, we investigate Greenland moisture source, global atmospheric composition, together with our Antarctic records, expanding the work of Guillevic et al. (2014) for multi-proxy Greenland and atmospheric composition records (Section 4.2).

4.1. Antarctic atmospheric circulation: aerosol and d-excess data

Here, we compare our three Antarctic $\delta^{18}\text{O}$ records to records of dust aerosols and d-excess in same ice cores. The second order parameter d-excess, expressed as $\delta\text{D}-8*\delta^{18}\text{O}$, is linked to evaporation conditions and shifts of moisture sources (e.g. Vimeux et al., 1999; Stenni et al., 2010). The level of high frequency variability (or noise) in d-excess profiles from TALDICE, EDC and EDML is a clear limitation to the detection of climatic signals. The d-excess is generally in anti-phase with $\delta^{18}\text{O}$ in EDC and EDML, but in phase at TALDICE (Fig. 7a). This supports the hypothesis that TALDICE has a different moisture source. More abrupt variations are recorded at TALDICE than EDC, while EDML d-excess shows generally smooth variations. Some abrupt shifts in TALDICE and EDC d-excess are detected at the start of the second phase of AIM 8 (plateau of EDML warming), and during Greenland abrupt warming. Similar features are also detected in one or the other core for earlier AIM events.

The signals depicted by the dust and aerosol records are more straightforward. To characterize changes in atmospheric mineral dust deposition (Lambert et al., 2012), we have used the dust flux from EDC and non-sea-salt calcium flux (hereafter nssCa^{2+}) from EDML and TALDICE. For EDC, analytical problems rule out the use of continuous flow nssCa^{2+} measurements for AIM 8 (Schüpbach et al., 2013). We therefore report the high resolution dust flux data from Lambert et al. (2012) which are strongly correlated to the flux of nssCa^{2+} in the other parts of EDC. AIM events are clearly recorded through changes in dust fluxes (Lambert et al., 2012; Schüpbach et al., 2013). This implies that AIM are associated with changes in atmospheric dust transport and/or changes in continental dust sources, located primarily in Southern Patagonia for East Antarctic cores during glacial periods (e.g. Basile et al., 1997; Delmonte et al., 2008; Wegner et al., 2012).

During AIM 8, the transition from phase 1 to phase 2 of Antarctic warming (start of the EDML plateau, change in warming rates at TALDICE and EDC) coincides with an abrupt decrease of dust fluxes (red arrows on Fig. 7a), a feature already observed by Ahn et al. (2012). The same pattern is observed in high resolution dust EDC data over AIM 12 but cannot be clearly detected in lower resolution nssCa^{2+} records from EDML and TALDICE. We attribute these abrupt shifts to changes in high latitude atmospheric circulation either reducing the uplift of dust in Patagonia or its atmospheric transport efficiency towards Antarctica. Using the more climatologically representative logarithmic scale to plot the high resolution dust flux of the Dome ice core (Fig. 7b and c), we can also identify some high frequency variations in the dust flux records over the warm phase of the AIM. Due to different resolutions and variability levels, it is not yet possible to detect whether sharp dust changes coincide with those of $\delta^{18}\text{O}$. The strong flux reduction occurring on vertical bar b for both AIM 8 and 12, i.e. at the beginning of the $\delta^{18}\text{O}$ plateau at EDML, is clearly visible. Moreover, we observe a “cold reversal” like pattern during the warming phases of both AIM 8 and 12 on the dust flux at EDC (marked R between bars b and c on Fig. 7b and c). Within the chronological uncertainties, this corresponds well to the slight cooling identified above on the high resolution profile of TALDICE (marked L between bars b and c on Fig. 7b and c).

Dust records therefore depict changes in atmospheric circulation during the transition from phase 1 to phase 2 of AIM 8 and AIM 12 that support fast atmospheric circulation reorganization taking place in addition to the general bipolar seesaw pattern. This pattern is less clearly imprinted in d-excess, and only visible for some of the d-excess data (EDC, TALDICE), during this transition and abrupt Greenland warming.

4.2. Bipolar climate and global atmospheric composition during AIM8

Here, we use the multi-proxy picture of Greenland and global atmospheric composition changes occurring during AIM 8 (Bock et al., 2010; Ahn et al., 2012; Chappellaz et al., 2013) transferred by Guillevic et al. (2014) on GICC05, together with the synchronized Antarctic records on AICC2012.

In Greenland, we use here the NEEM ice core, where a temperature reconstruction based on $\delta^{15}\text{N}$ is available for AIM8. We first stress the same patterns depicted in this temperature reconstruction and ice $\delta^{18}\text{O}$: the first long and stable cold phase (stadial) lasts ~1730 years (~39875 ka b 1950 to ~38145 ka b 1950 on the GICC05 – AICC2012 timescale), when an abrupt temperature increase of 10.4 ± 1.5 °C leads to a warm interstadial lasting more

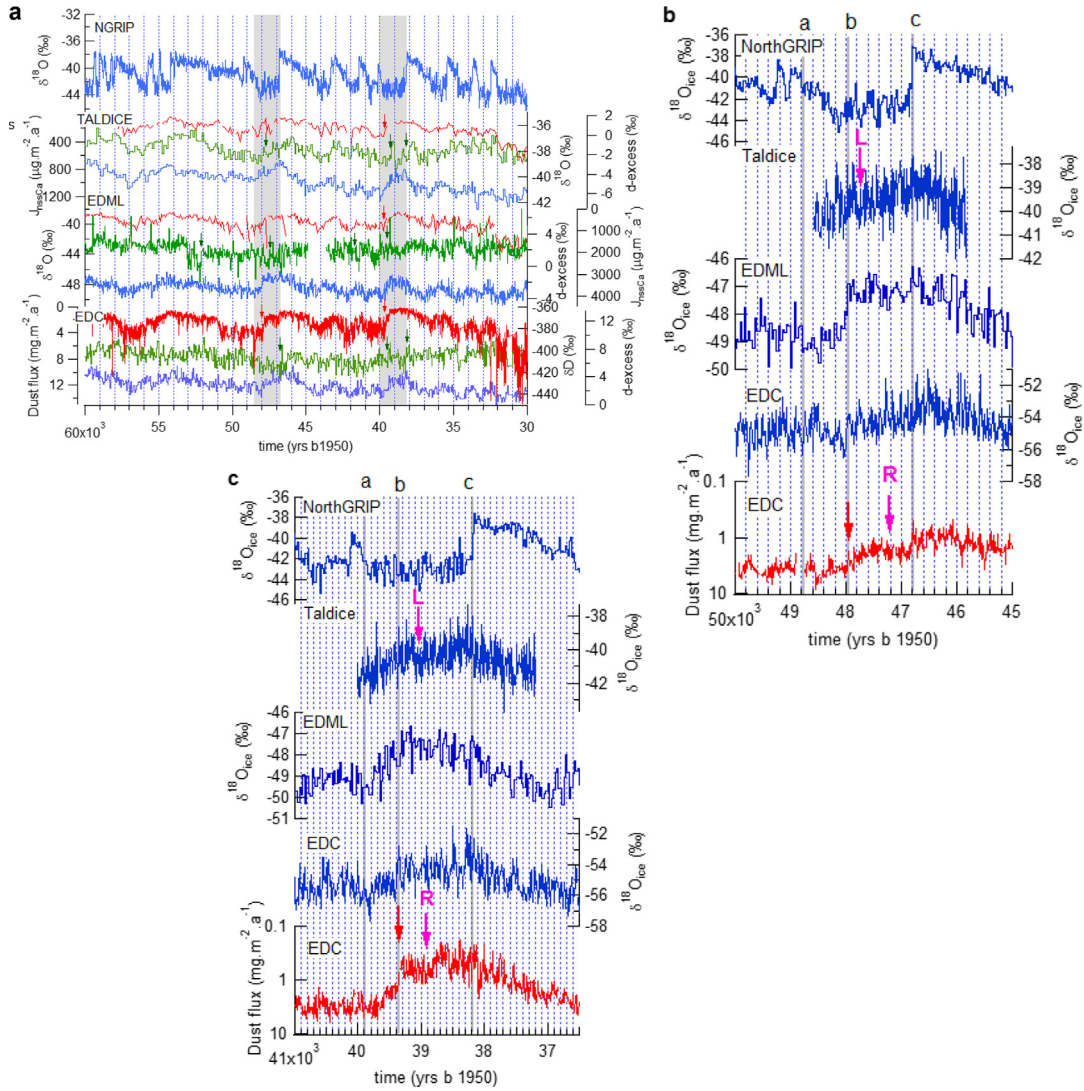


Fig. 7. a) comparison between water stable isotope records ($\delta^{18}\text{O}$ or deuterium) (blue), dust (EDC, on reversed axis) or nssCa^{2+} (TALDICE and EDML, on reversed axis) flux records (red) and d-excess records (green). Gray rectangles indicate GS 9 and 13 and red/green arrows the marked changes in dust flux/d-excess records. b) and c) comparison between high resolution water records at TALDICE and EDC with high resolution dust flux (running median of EDC dust flux at 10 cm resolution in logarithmic scale) at EDC for AIM 12 (b) and 8 (c). The red arrows is the same as in 7a and the pink arrows indicate the “cold reversal” like pattern identified in the dust record (R) and in the TALDICE water isotope records (L).

than 1200 years (Guillevic et al., 2013). While no sub-event can be identified during GS 9 in Greenland temperature reconstructions, more information emerges from proxy records which are sensitive to low latitude climate.

Continuous CH_4 measurements performed with a laser analyzer provide an unprecedented high resolution record at NEEM (Chappellaz et al., 2013), which unveils sub-millennial variations in CH_4 without a counter-part in Greenland ice $\delta^{18}\text{O}$. Several centuries after the onset of GS 9, at ~ 39.3 ka b 1950, when Greenland temperature is cold and stable, a small increase in CH_4 is detected and probably caused by changes in low latitude methane production (Dällenbach et al., 2000). Other parameters measured in Greenland ice cores, hence without chronological biases, confirm the occurrence of low latitude climatic shifts, several centuries after the onset of GS 9. Guillevic et al. (2014) show that NEEM ^{17}O -excess and $\delta^{18}\text{O}_{\text{atm}}$ remain stable over GIS 9 and the first part of GS 9, i.e. until 39.3 ka b 1950 on the AICC2012 timescale. While they do not record any variability at the time of abrupt Greenland cooling (at the beginning of GS 9), ^{17}O -excess ($\delta^{18}\text{O}_{\text{atm}}$) is showing a significant decrease (increase) at 39.3 ka b 1950, i.e. 600 years after the onset

of GS 9. ^{17}O -excess is defined by analogy to d-excess as the deviation of $\delta^{17}\text{O}$ from the $\delta^{17}\text{O}$ vs $\delta^{18}\text{O}$ meteoric water line as ^{17}O -excess = $\ln(\delta^{17}\text{O} + 1) - 0.528 \ln(\delta^{18}\text{O} + 1)$. In Greenland ice cores, it reflects changes in the evaporative conditions of the low latitudes oceanic moisture sources (Landais et al., 2012) so that an increase in ^{17}O -excess is directly linked to a decrease of relative humidity at evaporation. This is due to the influence of kinetic fractionation during evaporation of water (the drier the atmosphere, the stronger the kinetic fractionation and the higher the ^{17}O -excess). $\delta^{18}\text{O}_{\text{atm}}$ is an integrated tracer of changes in biosphere productivity and low latitudes water cycle (Bender et al., 1994b). Modifications of the low latitude hydrological cycle during DO events strongly influence the $\delta^{18}\text{O}$ of meteoric water in the low latitudes (Pausata et al., 2011). This signal is transmitted to $\delta^{18}\text{O}_{\text{atm}}$ through evapotranspiration in plants and photosynthesis. The strong similarities between the $\delta^{18}\text{O}_{\text{atm}}$ signal and the calcite $\delta^{18}\text{O}$ of low latitude speleothems also strongly suggests that $\delta^{18}\text{O}_{\text{atm}}$ is a direct tracer of low latitude hydrological cycle in the air trapped in ice core.

About 600 years after the onset of GS 9, the concomitant changes recorded in $\delta^{18}\text{O}_{\text{atm}}$, ^{17}O -excess and CH_4 reflect changes in

low latitude climate and water cycle, probably induced by a southward shift in the ITCZ occurring without fingerprint in Greenland temperature (Guillevic et al., 2014). Similarly, we suggest that a northward ITCZ shift explains the changes recorded at 38.6 ka b 1950, about 400 years before the abrupt Greenland temperature warming marking the end of GS 9. This encompasses an increase of ^{17}O -excess by ~ 20 ppm and a decrease of the δD of CH_4 by more than 10‰, consistent with changes in the low latitude precipitation isotopic composition (Bock et al., 2010).

A finer structure of changes within GS 9 is further supported by a highly resolved atmospheric CO_2 concentration obtained from the Antarctic Byrd ice (Ahn et al., 2012). The 20 ppm CO_2 increase during GS 9/AIM 8 occurs in two main steps, at ~ 39.3 ka b 1950 and at ~ 38.15 ka BP, punctuated by an intermediate smaller step at 38.6 ka b 1950 (Fig. 8).

The evolution of the Antarctic $\delta^{18}\text{O}$ records presents synchronicity with the sequence of changes within GS 9/AIM 8 (Fig. 5). The changes in CH_4 , CO_2 , $\delta^{18}\text{O}_{\text{atm}}$ and in ^{17}O -excess at 39.3 ka BP occur in phase (within age scale uncertainties) with the AIM 8 phase 1 and the increase to the EDML plateau (between vertical bars a and b, Figs. 6b, c and 8). We therefore identify simultaneous changes in low latitudes and Antarctic climate without any fingerprint in Greenland climate.

As in Guillevic et al. (2014) and as already observed from comparison of Greenland ice cores and lower latitudes marine cores (Sanchez Goni et al., 2008), we therefore conclude that Greenland climate during GS9 is decoupled from climate changes occurring at lower latitudes. During stadials, the onset of the iceberg rafted discharge appears delayed with respect to the collapse of the North Atlantic Deep Water (NADW) formation (Hall et al., 2006; Jonkers et al., 2010), itself often associated with the North Atlantic/Greenland surface temperature cooling. An explanation for this lag

has been suggested by Marcott et al. (2011) and Alvarez-Solas et al. (2013). They argue that the collapse of NADW formation, leading to the strong Greenland cooling, induces a slow sub-surface warming in North Atlantic, which would then trigger the iceberg discharge. Delays between abrupt North Atlantic cooling and the Heinrich event are therefore expected to reflect the duration required for sufficient heat accumulation in subsurface to trigger an iceberg discharge. Our structure is consistent with a lag between North Atlantic/Greenland cooling and a strong iceberg discharge which can then affect the atmospheric circulation at lower latitudes. Note that the recent modeling study of Roberts et al. (2014) shows that changes in topography following a strong iceberg discharge could also have a direct impact on North Atlantic climate. This is not obvious from Greenland records where no clear signature of Heinrich event has been detected (e.g. Guillevic et al., 2014).

We now summarize our findings for AIM 8. As predicted by the bipolar seesaw thermodynamical model, we observe (i) that the onset of Antarctic warming coincides with Greenland cooling, and (ii) that Greenland abrupt warming marks the beginning of Antarctic cooling. During GI 8, both Greenland and Antarctica are cooling in parallel. In addition to the seesaw pattern, the inflexion in Antarctic warming that we have identified during AIM8, most strongly recorded in EDML (start of a plateau) occurs in phase (within dating uncertainties) with low latitude climatic changes at 39.3 ka BP affecting sources of Greenland moisture as well as global atmospheric composition (CH_4 , CO_2 , $\delta^{18}\text{O}_{\text{atm}}$) and attributed to a southward ITCZ shift. While it has no fingerprint in Greenland temperature, this event marks the end of the first rapid increase in Antarctic temperature during AIM8, as well as rapid large-scale atmospheric circulation reorganizations from low latitudes (ITCZ southward shift) to high southern latitudes (as depicted by Antarctic dust and d-excess). We conclude that low latitudes climatic

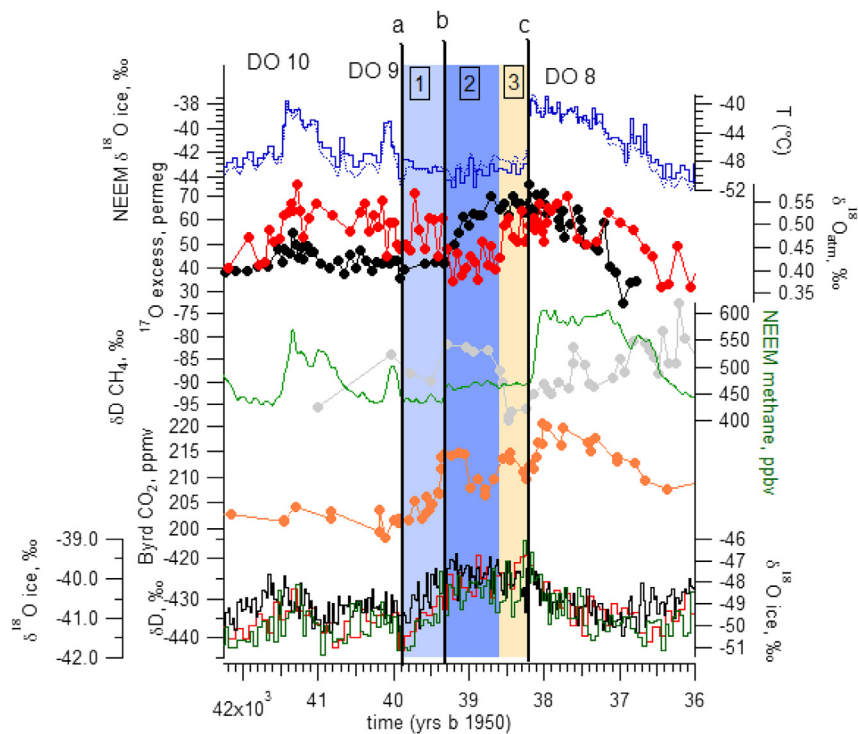


Fig. 8. Expanded from Guillevic et al. (2014). From top to bottom: NEEM $\delta^{18}\text{O}$ ice and reconstructed temperature (based on $\delta^{15}\text{N}$); NEEM ^{17}O -excess (red) and $\delta^{18}\text{O}_{\text{atm}}$ (black); NEEM methane concentration (Chappellaz et al., 2013, green) and NorthGRIP δD of CH_4 (Bock et al., 2010, gray), Byrd CO_2 (Ahn et al., 2012, orange) and Antarctic ice core $\delta^{18}\text{O}$ (black, EDML; red, TALDICE; green, EDC). All records have been synchronized on AICC2012. The vertical colored rectangles depict three phases within GS 9, identified in the Greenland records. The vertical bars a, b and c refer to the separation between phases of the AIM identified on Figs. 5 and 6.

changes during the course of a Greenland stadial complicate the classical picture of the bipolar seesaw. The decoupling between low and high latitudes during the Greenland stadial may be linked with a delayed iceberg discharge during the stadial due to subsurface warming as explained in the previous paragraph.

Simulations performed with coupled ocean-atmosphere models, forced by freshwater hosing in the North Atlantic in order to depict a millennial scale variability, show some decoupling between Greenland temperature (mostly affected by surface conditions, e.g. sea-ice) and AMOC strength. [Otto-Bliesner and Brady \(2010\)](#) performed an idealized experiment where a massive freshwater flux (1 Sv) is applied during 100 years and obtained a gradual AMOC reduction within 100 years and a slow recovery over the next 500 years. The associated simulated Greenland temperature shows an abrupt cooling of about 6 °C at the beginning of the freshwater flux in response to very fast sea-ice area increase in the North Hemisphere and a slow return to initial conditions following the AMOC response. The simulated temperature response is anti-phased with AMOC in the South Atlantic and more gradual in the Antarctic regions. In another study investigating the role of realistic geographic freshwater forcing in a coupled climate model, [Roche et al. \(2010\)](#) found also a slight decoupling between simulated Greenland temperatures and AMOC strength, the latter being delayed when the AMOC is close to a complete shutdown, while the simulated temperature in Greenland is more sensitive to surface conditions in the Nordic Seas. In particular, they showed that the occurrence of deep convection in the Nordic Seas is a prime control on sea-ice extent, recovery time of the AMOC and Greenland temperature anomalies. Finally [Roche et al. \(2010\)](#) found that the Antarctic warming is weak and delayed with respect to the peak Greenland cooling. Even if the last feature is not obvious in the ice core data, it shows that the modeled climatic evolution in response to freshwater fluxes can thus be different from the simple bipolar seesaw idealized by [Stocker and Johnsen \(2003\)](#).

5. Conclusions and perspectives

Despite uncertainties associated with chronologies of East Antarctic ice cores, the AICC2012 approach provides an accurate framework to investigate the bipolar patterns of glacial climate variability at the millennial time scale, and at the multi-centennial time scale when sufficient stratigraphic links are available, such as for the period close to the Laschamp event.

Common features of Antarctic climate variability are evidenced in a $\delta^{18}\text{O}$ stack record. Precise synchronization of the different ice core records reveals regional differences. At EDML, AIM 8 and AIM 12 are marked by a fast $\delta^{18}\text{O}$ increase, followed by a plateau, while TALDICE and EDC depict a more gradual increase, with reduced rate of warming when EDML reaches this plateau. High resolution data from EDC and TALDICE further depict an optimum at this inflexion point and sharp warm events at EDC associated with the warm AIM phases and inflexion points during the Antarctic warming.

Large scale features of Antarctic $\delta^{18}\text{O}$ variations are consistent with the overall seesaw pattern associated with changes in Atlantic ocean circulation modulated by the inertia of the southern Ocean, such as an overall warming during the Greenland cold phases, ending when Greenland is abruptly warming. However, sub-millennial features of Antarctic variability occur without a Greenland counterpart. This is for instance the case for the two step patterns occurring during the warming phase of AIM 8 and AIM 12. Antarctic ice core data related to dust deposition and moisture origin (d-excess) reveal parallel changes in high latitude atmospheric circulation, with a very clear signal in dust.

During the warming phase of AIM 8, Greenland temperature is cold and stable, while changes in Greenland moisture origin and

global atmospheric composition suggest reorganizations of low latitude atmospheric circulation, probably associated with a southward ITCZ shift, in parallel with the inflexion identified in the Antarctic ice cores.

During long stadials, there is no fingerprint of Heinrich events in Greenland temperature but a more complex pattern in the bipolar structure of events than described in the conceptual bipolar seesaw thermodynamical model. We suggest that, during these long cold phases, Greenland temperature is decoupled from changes in AMOC and changes in low latitude atmospheric circulation. Our Antarctic high resolution data suggest fast teleconnections between changes in low latitude atmospheric circulation and Antarctic temperature, consistent with recent observations ([Ding et al., 2011](#)). The bipolar seesaw concept therefore does not correctly reflect the complexity of processes at play.

In this study, we thus challenge (i) reconstructions of past Greenland temperature based on the inversion of the bipolar seesaw model using long Antarctic climate records ([Barker et al., 2011](#)), and (ii) the use of Greenland ice core records as a reference for the timing of climatic changes in North Atlantic during the Last Glacial period. During cold phases, the wide extent of sea ice around Greenland probably isolates this region from climate changes occurring at lower latitudes.

Acknowledgments

This work is a contribution to the European Project for Ice Coring in Antarctica (EPICA), a joint European Science Foundation/European Commission scientific program, funded by the EU and by national contributions from Belgium, Denmark, France, Germany, Italy, the Netherlands, Norway, Sweden, Switzerland and the United Kingdom. The main logistic support was provided by IPEV and PNRA (at Dome C) and AWI (at Dronning Maud Land). The Talos Dome Ice core Project (TALDICE), a joint European programme, is funded by national contributions from Italy, France, Germany, Switzerland and the UK. Primary logistical support was provided by PNRA at Talos Dome. F. Lambert acknowledges support by Project CONICYT/FONDAP 15110009 and NC120066. This work has benefited from supports from the French ANR (Agence Nationale de Recherche), the foundation Ars et Cuttoli and the ERC program COMBINISO (306045). The authors thank the reviewer for his important inputs that improved the quality of the final manuscript.

References

- [Adkins, J.F., 2013. The role of deep ocean circulation in setting glacial climates. *Paleoceanography* 28 \(3\), 539–561.](#)
- [Ahn, J., Brook, E., Schmittner, A., Kreutz, K., 2012. Abrupt change in atmospheric CO₂ during the last ice age. *Geophys. Res. Lett.* 39, L18771. <http://dx.doi.org/10.1029/2012GL053018>.](#)
- [Alvarez-Solas, J., Ramstein, G., 2011. On the triggering mechanism of Heinrich events. *Proc. Natl. Acad. Sci. U. S. A.* 108, E1359–E1360. <http://dx.doi.org/10.1073/pnas.1116575108>.](#)
- [Alvarez-Solas, J., Robinson, A., Montoya, M., Ritz, C., 2013. Iceberg discharges of the last glacial period driven by oceanic circulation changes. *Proc. Natl. Acad. Sci. U. S. A.* <http://dx.doi.org/10.1073/pnas.1306622110>.](#)
- [Anderson, R.F., Ali, S., Bradtmiller, L.I., Nielsen, S.H.H., Fleisher, M.Q., Anderson, B.E., Burckle, L.H., 2009. Wind-driven upwelling in the Southern Ocean and the deglacial rise in atmospheric CO₂. *Science* 323, 1443–1448.](#)
- [Arzel, O., Colin de Verdière, A., England, M.H., 2010. The role of oceanic heat transport and wind-stress forcing in abrupt millennial-scale climate transitions. *J. Clim.* 23, 2233–2256.](#)
- [Arzel, O., England, M.H., Colin de Verdière, A., Huck, T., 2012. Abrupt millennial variability and interdecadal-stadial oscillations in a global coupled model: sensitivity to the background climate state. *Clim. Dyn.* 39, 259–275.](#)
- [Barker, S., Diz, P., Vautravers, M.J., Pike, J., Knorr, G., Hall, I.R., Broecker, W.S., 2009. Interhemispheric Atlantic seesaw response during the last deglaciation. *Nature* 457, 1097–1102.](#)

- Barker, S., Knorr, G., Edwards, R.L., Parrenin, F., Putnam, A.E., Skinner, L.C., Wolff, E., Ziegler, M., 2011. 800,000 years of abrupt climate variability. *Science* 334 (6054), 347–351.
- Basile, I., Grousset, F.E., Revel, M., Petit, J.R., Biscaye, P.E., Barkov, N.I., 1997. Patagonian origin of glacial dust deposited in East Antarctica (Vostok and Dome C) during glacial stages 2, 4 and 6. *Earth Planet. Sci. Lett.* 146, 573–589. [http://dx.doi.org/10.1016/S0012-821X\(96\)00255-5](http://dx.doi.org/10.1016/S0012-821X(96)00255-5).
- Bazin, L., Landais, A., Lemieux-Dudon, B., Toyé Mahamadou Kele, H., Veres, D., Parrenin, F., Martinerie, P., Ritz, C., Capron, E., Lipenkov, V., Loutre, M.-F., Raynaud, D., Vinther, B., Svensson, A., Rasmussen, S.O., Severi, M., Blunier, T., Leuenberger, M., Fischer, H., Masson-Delmotte, V., Chappellaz, J., Wolff, E., 2013. An optimized multi-proxy, multi-site Antarctic ice and gas orbital chronology (AICC2012): 120–800 ka. *Clim. Past* 9, 1715–1731. <http://dx.doi.org/10.5194/cp-9-1715-2013>.
- Bazin, L., Lemieux-Dudon, B., Landais, A., Guillevic, M., Kindler, P., Parrenin, F., Martinerie, P., 2014. Optimisation of glaciological parameters for ice core chronology by implementing counted layers between identified depth levels. *Clim. Past Discuss.* 10, 3585–3616.
- Bender, M., Sowers, T., Dickson, M.-L., Orcharto, J., Grootes, P., Mayewski, P., Meese, D., 1994a. Climate connections between Greenland and Antarctica during the last 100,000 years. *Nature* 372, 663–666.
- Bender, M., Sowers, T., Labeyrie, L., 1994b. The Dole effect and its variations during the last 130,000 years as measured in the Vostok ice core. *Global Biogeochem. Cycles* 8, 363–376. <http://dx.doi.org/10.1029/94GB00724>.
- Bentley, M.J., Fogwill, C.J., Le Brocq, A.M., Hubbard, A.L., Sugden, D.E., Dunai, T., Freeman, S.P.H.T., 2010. Deglacial history of the West Antarctic Ice Sheet in the Weddell Sea embayment: constraints on past ice volume change. *Geology* 38, 411–414.
- Blunier, T., Brook, E.J., 2001. Timing of millennial-scale climate change in Antarctica and Greenland during the last glacial period. *Science* 291, 109–112.
- Blunier, T., Chappellaz, J., Schwander, J., Dällenbach, A., Stauffer, B., Stocker, T.F., Raynaud, D., Jouzel, J., Clausen, H.B., Hammer, C.U., Johnsen, S.J., 1998. Asynchrony of Antarctic and Greenland climate change during the last glacial period. *Nature* 394, 739–743.
- Bock, M., Schmitt, J., Möller, L., Spahni, R., Blunier, T., Fischer, H., 2010. Hydrogen isotopes preclude marine hydrate CH₄ emissions at the onset of Dansgaard-Oeschger events. *Science* 10 (328), 1686–1689. <http://dx.doi.org/10.1126/science.1187651>.
- Bond, G., Heinrich, H., Broecker, W., Labeyrie, L., McManus, J., Andrews, J., Huon, S., Jantschik, R., Clasen, S., Simet, C., 1992. Evidence for massive discharges of icebergs into the North Atlantic Ocean during the last glacial period. *Nature* 360, 245–249.
- Broccoli, A.J., Dahl, K.A., Stouffer, R.J., 2006. The response of the ITCZ to Northern Hemisphere cooling. *Geophys. Res. Lett.* 33, L01702. <http://dx.doi.org/10.1029/2005GL024546>.
- Broecker, W.S., 1991. The great ocean conveyor. *Oceanography* 4, 79–89.
- Broecker, W.S., 1998. Paleocirculation during the last deglaciation: a bipolar seesaw? *Paleoceanography* 13, 119–121.
- Broecker, W.S., Bond, G.C., Klas, M., Clark, E., McManus, J.F., 1992. Origin of the northern Atlantic's Heinrich events. *Clim. Dyn.* 6, 265–273.
- Buiron, D., Chappellaz, J., Stenni, B., Frezzotti, M., Baumgartner, M., Capron, E., Landais, A., Lemieux-Dudon, B., Masson-Delmotte, V., Montagnat, M., Parrenin, F., Schilt, A., 2011. TALDICE-1 age scale of the Talos Dome deep ice core, East Antarctica. *Clim. Past* 7, 1–16. <http://dx.doi.org/10.5194/cp-7-1-2011>.
- Buiron, D., Stenni, B., Chappellaz, J., Landais, A., Baumgartner, M., Bonazza, M., Capron, E., Frezzotti, M., Kageyama, M., Lemieux-Dudon, B., Masson-Delmotte, V., Parrenin, F., Schilt, A., Selmo, E., Severi, M., Swingedouw, D., Udisti, R., 2012. Regional imprints of millennial variability during the MIS 3 period around Antarctica. *Quat. Sci. Rev.* 48, 99–112.
- Buizert, C., Gkinis, V., Severinghaus, J.P., He, F., Lecavalier, B.S., Kindler, P., Leuenberger, M., Carlson, E., Vinther, B., Masson-Delmotte, V., White, J.W.C., Liu, Z., Otto-Bliesner, B., Brook, E.J., 2014. Greenland temperature response to climate forcing during the Last Deglaciation. *Science* 345, 1177–1180. <http://dx.doi.org/10.1126/science.1254961>.
- Cane, M., Clement, A.C., 1999. A Role for the Tropical Pacific Coupled Ocean-atmosphere System on Milankovitch and Millennial Timescales. Part I: a Modeling Study of Tropical Pacific Variability, Mechanism of Global Climate Change at Millennial Time Scales. In: *Geophysical Monograph*, 112. American Geophysical Union.
- Capron, E., Landais, A., Chappellaz, J., Schilt, A., Buiron, D., Masson-Delmotte, V., Jouzel, J., Lemieux-Dudon, B., Govin, A., Loulergue, L., Leuenberger, M., Mayer, H., Oerter, H., Dahl-Jensen, D., Johnsen, S., Stenni, B., 2010a. Millennial-scale climatic variability over the last glacial period: Greenland-Antarctic sequences of events over Marine Isotopic Stage (MIS) 5 compared to MIS 3. *Clim. Past* 6, 1–49.
- Capron, E., Landais, A., Lemieux, B., Schilt, A., Loulergue, L., Buiron, D., Chappellaz, J., Masson-Delmotte, V., Dahl-Jensen, D., Johnsen, S., Leuenberger, M., Oerter, H., 2010b. Synchronising EDML and NorthGRIP ice cores using $\delta^{18}\text{O}$ of atmospheric oxygen ($\delta^{18}\text{O}_{\text{atm}}$) and CH₄ measurements over MIS5 (80–123 kyr). *QSR* 1–2, 222–234.
- Capron, E., Landais, A., Chappellaz, J., Buiron, D., Fischer, H., Johnsen, S., Jouzel, J., Leuenberger, M., Masson-Delmotte, V., Stocker, T.F., 2012. A global picture of the first abrupt climatic event occurring during the last glacial inception. *GRL*. <http://dx.doi.org/10.1029/2012GL026566>.
- Carlson, A.E., Winsor, K., 2012. Northern Hemisphere ice-sheet responses to past climate warming. *Nat. Geosci.* 5, 607–613.
- Chappellaz, J., Blunier, T., Raynaud, D., Barnola, J., Schwander, J., Stauffer, B., 1993. Synchronous changes in atmospheric CH₄ and Greenland climate between 40 and 8 kyr BP. *Nature* 366, 443–445.
- Chappellaz, J., Stowasser, C., Blunier, T., Baslev-Clausen, D., Brook, E.J., Dallmayr, R., Fain, X., Lee, J.E., Mitchell, L.E., Pascual, O., Romanini, D., Rosen, J., Schüpbach, S., 2013. High-resolution glacial and deglacial record of atmospheric methane by continuous flow and laser spectrometer analysis along the NEEM ice core. *Clim. Past* 9, 2579–2593. <http://dx.doi.org/10.5194/cp-9-2579-2013>.
- Clark, P.U., Dyke, A.S., Shakun, J.D., Carlson, A.E., Clark, J., Wohlfarth, B., Mitrovica, J.X., Hostetler, S.W., McCabe, A.M., 2009. The Last Glacial Maximum. *Science* 325, 710–714.
- Clement, A.C., Peterson, L.C., 2008. Mechanisms of abrupt climate change of the last glacial period. *Rev. Geophys.* 46, RG4002. <http://dx.doi.org/10.1029/2006RG000204>.
- Colin de Verdière, A., te Raa, L., 2010. Weak oceanic heat transport as a cause of the instability of glacial climates. *Clim. Dyn.* 35, 1237–1256.
- Dahl, K.D., Oppo, D.W., Eglinton, T.L., Hughen, K.A., Curry, W.B., Sirocko, F., 2005. Terrigenous plant wax inputs to the Arabian sea: implications for the reconstruction of winds associated with the Indian Monsoon. *Geochim. Cosmochim. Acta* 69, 2547–2558.
- Dällenbach, A., Blunier, T., Flückiger, J., Stauffer, B., Chappellaz, J., Raynaud, D., 2000. Changes in the atmospheric CH₄ gradient between Greenland and Antarctica during the Last Glacial and the transition to the Holocene. *Geophys. Res. Lett.* 27, 1005–1008.
- Dansgaard, W., Johnsen, S.J., Clausen, H.B., Dahl-Jensen, D., Gundestrup, N.S., Hammer, C.U., Hvidberg, C.S., Steffensen, J.P., Sveinbjörnsdóttir, A.E., Jouzel, J., Bond, G., 1993. Evidence for general instability of past climate from a 250-kyr ice-core record. *Nature* 364, 218–220.
- Delmonte, B., Andersson, P.S., Hansson, M., Schöberg, H., Petit, J.R., Basile-Doelsch, I., Maggi, V., 2008. Aeolian dust in East Antarctica (EPICA-Dome C and Vostok): provenance during glacial ages over the last 800 kyr. *Geophys. Res. Lett.* 35, 2–7. <http://dx.doi.org/10.1029/2008GL033382>.
- Deschamps, P., Durand, N., Bard, E., Hamelin, B., Camoin, G., Thomas, A.L., Henderson, G.M., Okuno, J., Yokoyama, Y., 2012. Ice-sheet collapse and sea-level rise at the Bolling warming 14,600 years ago. *Nature* 483, 559–564.
- Ding, Q., Steig, E.J., Battisti, D.S., Küttel, M., 2011. Winter warming in West Antarctica caused by central tropical Pacific warming. *Nat. Geosci.* 4, 398–403. <http://dx.doi.org/10.1038/ngeo1129>.
- Elliot, M., Labeyrie, L., Duplessy, J.C., 2002. Changes in North Atlantic deep-water formation associated with the Dansgaard-Oeschger temperature oscillations (10–60 ka). *Quat. Sci. Rev.* 21, 1153–1165.
- EPICA Community Members, 2006. One-to-one coupling of glacial climate variability in Greenland and Antarctica. *Nature* 444, 195–198. <http://dx.doi.org/10.1038/nature05301>.
- Ganopolski, A., 2003. Glacial integrative modelling. *Philos. Trans. R. Soc. A* 361, 1871–1884.
- Ganopolski, A., Rahmstorf, S., 2001. Rapid changes of glacial climate simulated in a coupled climate model. *Nature* 409, 153–158.
- Ganopolski, A., Calov, R., Claussen, M., 2010. Simulation of the last glacial cycle with a coupled climate ice-sheet model of intermediate complexity. *Clim. Past* 6, 229–244. <http://dx.doi.org/10.5194/cp-6-229-2010>.
- Golledge, N.R., Menviel, L., Carter, L., Fogwill, C.J., England, M.H., Cortese, G., Levy, R.H., 2014. Antarctic contribution to meltwater pulse 1A from reduced Southern Ocean overturning. *Nat. Commun.* 5. Article number: 5107.
- Goujon, C., Barnola, J.M., Ritz, C., 2003. Modeling the densification of polar firn including heat diffusion: application to close-off characteristics and gas isotopic fractionation for Antarctica and Greenland sites. *J. Geophys. Res.* 108, 101–1018.
- Groegoire, L.J., Payne, A.J., Valdes, P.J., 2012. Deglacial rapid sea level rises caused by ice-sheet saddle collapses. *Nature* 487 (7406), 219–222. <http://dx.doi.org/10.1038/nature11257>.
- Grootes, P.M., Stulver, M., White, J.W.C., Johnsen, S., Jouzel, J., 1993. Comparison of oxygen isotope records from the GISP2 and GRIP Greenland ice cores. *Nature* 366, 552–554.
- Grousset, F.E., Labeyrie, L., Sinko, J.A., Cremer, M., Bond, G., Duprat, J., Cortijo, E., Huon, S., 1993. Patterns of ice rafted detritus in the glacial North Atlantic (40–55°N). *Paleoceanography* 8 (2), 175–192.
- Guillevic, M., Bazin, L., Landais, A., Kindler, P., Orsi, A., Masson-Delmotte, V., Blunier, T., Buchardt, S.L., Capron, E., Leuenberger, M., Martinerie, P., Prié, F., Vinther, B.M., 2013. Spatial gradients of temperature, accumulation and $\delta^{18}\text{O}$ -ice in Greenland over a 5 series of Dansgaard-Oeschger events. *Clim. Past* 9, 1029–1051. <http://dx.doi.org/10.5194/cp-9-1029-2013>.
- Guillevic, M., Bazin, L., Landais, A., Stowasser, C., Masson-Delmotte, V., Blunier, T., Eynaud, F., Falourd, S., Michel, E., Minster, B., Popp, T., Prié, F., Vinther, B.M., 2014. Multi-proxy fingerprint of Heinrich event 4 in Greenland ice core records. *Clim. Past Discuss.* 10, 1179–1222. <http://dx.doi.org/10.5194/cpd-10-1179-2014>.
- Guillou, H., Singer, B.S., Laj, C., Kissel, C., Scailliet, S., Jicha, B.R., 2004. On the age of the Laschamp geomagnetic excursion. *Earth Planet. Sci. Lett.* 227, 331–343.
- Hall, I.R., Moran, S.B., Zahn, R., Knutz, P.C., Shen, C.C., Edwards, R.L., 2006. Accelerated drawdown of meridional overturning in the late-glacial Atlantic triggered by transient pre-H event freshwater perturbation. *Geophys. Res. Lett.* 33, L16616. <http://dx.doi.org/10.1029/2006GL026239>.
- Heinrich, H., 1988. Origin and consequences of cyclic ice rafting in the Northeast Atlantic Ocean during the past 130,000 years. *Quat. Res.* 29, 142–152.

- Hemming, S.R., 2004. Heinrich events: massive late Pleistocene detritus layers of the North Atlantic and their global climate imprint. *Rev. Geophys.* 42, RG1005. <http://dx.doi.org/10.1029/2003RG000128>.
- Hörhold, M.W., Laepple, T., Freitag, J., Bigler, M., Fischer, H., Kipfstuhl, S., 2012. On the impact of impurities on the densification of polar firn. *Earth Planet. Sci. Lett.* 325–326, 93–99. <http://dx.doi.org/10.1016/j.epsl.2011.12.022>.
- Huber, C., Leuenberger, M., Spahni, R., Flückiger, J., Schwander, J., Stocker, T., Johnsen, S., Landais, A., Jouzel, J., 2006. Isotope calibrated Greenland temperature record over Marine Isotope Stage 3 and its relation to CH₄. *Earth Planet. Sci. Lett.* 243, 504–519.
- Jonkers, L., Moros, M., Prins, M.A., Dokken, T., Dahl, C.A., Dijkstra, N., Perner, K., Brummer, G.-J.A., 2010. A reconstruction of sea surface warming in the northern North Atlantic during MIS 3 ice-rafting events. *Quat. Sci. Rev.* 29, 1791–1800.
- Jouzel, J., Lorius, C., Johnsen, S.J., Grootes, P., 1994. Climate instabilities – Greenland and Antarctic records. *C. R. l'Acad. Sci. série II* 319 (1), 65–77.
- Jouzel, J., Masson-Delmotte, V., Cattani, O., Dreyfus, G., Falourd, S., Hoffmann, G., Minster, B., Nouet, J., Barnola, J.-M., Chappellaz, J., Fischer, H., Gallet, J.C., Johnsen, S.J., Leuenberger, M., Loulergue, L., Luethi, D., Oerter, H., Parrenin, F., Raisbeck, G., Raynaud, D., Schilt, A., Schwander, J., Selmo, E., Souchez, R., Spahni, R., Stauffer, B., Steffensen, J.P., Stenni, B., Stocker, T., Tison, J.-L., Werner, M., Wolff, E., 2007. Orbital and millennial Antarctic climate variability over the past 800,000 years. *Science* 317 (5839), 793–797. <http://dx.doi.org/10.1126/science.1141038>.
- Jouzel, J., Delaigle, G., Landais, A., Masson-Delmotte, V., Risi, C., Vimeux, F., 2013. Water isotopes as tools to document oceanic sources of precipitation. *Water Resour. Res.* 49 (11), 7469–7486. <http://dx.doi.org/10.1002/2013WR013508>.
- Kageyama, M., Paul, A., Roche, D.M., van Meerbeeck, C.J., 2010. Modelling glacial climatic millennial-scale variability related to changes in the Atlantic meridional overturning circulation: a review. *Quat. Sci. Rev.* 29, 2931–2956.
- Kageyama, M., Merkel, U., Otto-Bliesner, B., Prange, M., Abe-Ouchi, A., Lohmann, G., Ohgaito, R., Roche, D.M., Singarayer, J., Swingedouw, D., Zhang, X., 2013. Climatic impacts of fresh water hosing under Last Glacial Maximum conditions: a multi-model study. *Clim. Past* 9, 935–953.
- Kilfeather, A.A., Cofaigh, C.O., Lloyd, J.M., Dowdeswell, J.A., Xu, S., Moreton, G., 2011. Ice-stream retreat and ice-shelf history in Marguerite Trough, Antarctic Peninsula: sedimentological and foraminiferal signatures. *Geol. Soc. Am. Bull.* 123, 997–1015.
- Kindler, P., Guillevic, M., Baumgartner, M., Schwander, J., Landais, A., Leuenberger, M., 2014. Temperature reconstruction from 10 to 120 kyr b2k from the NGRIP ice core. *Clim. Past* 10, 887–902. <http://dx.doi.org/10.5194/cp-10-887-2014>.
- Köhler, P., Knorr, G., Buiron, D., Lourantou, A., Chappellaz, J., 2011. Abrupt rise in atmospheric CO₂ at the onset of the Bølling/Allerød: in-situ ice core data versus true atmospheric signals. *Clim. Past* 7, 473–486. <http://dx.doi.org/10.5194/cp-7-473-2011>.
- Krebs, U., Timmermann, A., 2007. Tropical air-sea interactions accelerate the recovery of the Atlantic Meridional overturning circulation after a major shutdown. *J. Clim.* 20, 4940–4956.
- Labeyrie, L., Leclaire, H., Waelbroeck, C., Cortijo, E., Duplessy, J.-C., Vidal, L., Elliot, M., Le Coat, B., Auffret, G., 1999. Temporal variability of the surface and deep waters of the North West Atlantic Ocean at orbital and millennial scales. *Mechanisms of Global Climate Change at Millennial Time Scales*. In: Clark, P.U., Webb, R.S., Keigwin, D. (Eds.), *Geophys. Monogr. Ser.*, vol. 112. AGU, Washington D. C., pp. 77–98.
- Lambert, F., Bigler, M., Steffensen, J.P., Hutterli, M., Fischer, H., 2012. Centennial mineral dust variability in high-resolution ice core data from Dome C, Antarctica. *Clim. Past* 8, 609–623. <http://dx.doi.org/10.5194/cp-8-609-2012>.
- Landais, A., Barnola, J.M., Kawamura, K., Caillon, N., Delmotte, M., Van Ommen, T., Dreyfus, G., Jouzel, J., Masson-Delmotte, V., Minster, B., Freitag, J., Leuenberger, M., Schwander, J., Huber, C., Etheridge, D., Morgan, V., 2006. Firn-air d₁₅N in modern polar sites and glacial-interglacial ice: a model-data mismatch during glacial periods in Antarctica? *Quat. Sci. Rev.* 25 (1–2), 49–62.
- Landais, A., Dreyfus, G., Capron, E., Masson-Delmotte, V., Sanchez-Goni, M., Desprat, S., Hoffmann, G., Jouzel, J., Leuenberger, M., Johnsen, S., 2007. What drives the millennial and orbital variations of d₁₈O_{atm}? *Quat. Sci. Rev.* 29, 235–246. <http://dx.doi.org/10.1016/j.quascirev.2009.07.005>.
- Landais, A., Steen-Larsen, H., Guillevic, M., Masson-Delmotte, V., Vinther, B., Winkler, R., 2012. Triple isotopic composition of oxygen in surface snow and water vapor at NEEM (Greenland). *Geochim. Cosmochim. Acta* 77, 304–316. <http://dx.doi.org/10.1016/j.gca.2011.11.022>.
- Lemieux-Dudon, B., Blayo, E., Petit, J.R., Waelbroeck, C., Svensson, A., Ritz, C., Barnola, J.M., Narcisi, B.M., Parrenin, F., 2010. Consistent dating for Antarctic and Greenland ice cores. *Quat. Sci. Rev.* 29, 8–20.
- Li, C., Battisti, D.S., Schrag, D.P., Tziperman, E., 2005. Abrupt climate shifts in Greenland due to displacements of the sea ice edge. *Geophys. Res. Lett.* 32 <http://dx.doi.org/10.1029/2005GL023492>.
- Li, C., Battisti, D.S., Bitz, C.M., 2010. Can North Atlantic sea ice anomalies account for Dansgaard-Oeschger climate signals? *J. Clim.* 23, 5457–5475.
- Liu, Z., Otto-Bliesner, B., He, F., Brady, E., Clark, P., Lynch-Steiglitz, J., Carlson, A., Curry, W., Brook, E., Jacob, R., Erickson, D., Kutzbach, J., Cheng, J., 2009. Transient simulation of Last Deglaciation with a new mechanism for Bolling-Allerød warming. *Science* 325, 310–314.
- Loulergue, L., 2007. Contraintes chronologiques et biogéochimiques grace au méthane dans la glace naturelle: une application aux forages du projet EPICA, 2007 (Ph.D. thesis). UJF, France.
- Loulergue, L., Parrenin, F., Blunier, T., Barnola, J.-M., Spahni, R., Schilt, A., Raisbeck, G., Chappellaz, J., 2007. New constraints on the gas age-ice age difference along the EPICA ice cores, 0–50 kyr. *Clim. Past* 3, 527–540. <http://dx.doi.org/10.5194/cp-3-527-2007>.
- MacAyeal, D.R., 1993. Binge/purge oscillations of the Laurentide ice sheet as a cause of the North Atlantic's Heinrich events. *Paleoceanography* 8 (6), 775–784.
- Mackintosh, A., Golledge, N., Domack, E., Dunbar, R., Leventer, A., White, D., Pollard, D., DeConto, R., Fink, D., Zwart, D., Gore, D., Lavoie, C., 2011. Retreat of the East Antarctic ice sheet during the last glacial termination. *Nat. Geosci.* 4, 95–202.
- Marcott, S.A., Clark, P.U., Padman, L., Klinkhammer, G.P., Springer, S.R., Liu, Z., Otto-Bliesner, B.L., Carlson, A.E., Ungerer, A., Padman, J., He, F., Cheng, J., Schmittner, A., 2011. Ice-shelf collapse from subsurface warming as a trigger for Heinrich events. *Proc. Natl. Acad. Sci. U. S. A.* 108, 13415–13419. <http://dx.doi.org/10.1073/pnas.1104772108>.
- Marshall, S.J., Clarke, G.K.C., 1997. A continuum mixture model of ice stream thermomechanics in the Laurentide Ice Sheet, 2. Application to the Hudson Strait Ice Stream. *J. Geophys. Res.* 102, 20,615–20,638.
- Martrat, B., Grimalt, J.O., Shackleton, N.J., de Abreu, L., Hutterli, M., Stocker, T., 2007. Four climate cycles of recurring deep and surface water destabilizations on the Iberian margin. *Science* 317, 502–507.
- McManus, J.F., Anderson, R., Broecker, W.S., Fleisher, M.Q., Higgins, S.M., 1998. Radiometrically determined sedimentary fluxes in the sub-polar North Atlantic during the last 140,000 years. *Earth Planet. Sci. Lett.* 155, 29–43.
- McManus, J.F., Oppo, D.W., Cullen, J.L., 1999. A 0.5-million-year record of millennial-scale climate variability in the North Atlantic. *Science* 283, 971–975.
- Meissner, K.J., Eby, M., Weaver, A.J., Saenko, O.A., 2006. CO₂ threshold for millennial-scale oscillations in the climate system: implications for global warming scenarios. *Clim. Dyn.* 30, 161–174.
- Menviel, L., Timmermann, A., Friedrich, T., England, M.H., 2014. Hindcasting the continuum of Dansgaard-Oeschger variability: mechanisms, patterns and timing. *Clim. Past* 10, 63–77. <http://dx.doi.org/10.5194/cp-10-63-2014>.
- NEEM Community Members, 2013. Eemian interglacial reconstructed from a Greenland folded ice core. *Nature* 493, 489–494.
- North Greenland Ice Core Project Members, 2004. High-resolution record of Northern Hemisphere climate extending into the last interglacial period. *Nature* 431, 147–151.
- Otto-Bliesner, B.L., Brady, E.C., 2010. The sensitivity of the climate response to the magnitude and location of freshwater forcing: last glacial maximum experiments. *Quat. Sci. Rev.* 29, 56–73. <http://dx.doi.org/10.1016/j.quascirev.2009.07.004>.
- Paillard, D., Labeyrie, L.D., 1994. Role of the thermohaline circulation in the abrupt warming after Heinrich events. *Nature* 372, 162–164.
- Parrenin, F., Petit, J.-R., Masson-Delmotte, V., Wolff, E., Basile-Doelsch, I., Jouzel, J., Lipenkov, V., Rasmussen, S.O., Schwander, J., Severi, M., Udisti, R., Veres, D., Vinther, B.M., 2012a. Volcanic synchronisation between the EPICA Dome C and Vostok ice cores (Antarctica) 0–145 kyr B. *Clim. Past* 8, 1031–1045.
- Parrenin, F., Barker, S., Blunier, T., Chappellaz, J., Jouzel, J., Landais, A., Masson-Delmotte, V., Schwander, J., Veres, D., 2012b. On the gas-ice depth difference (Adepth) along the EPICA Dome C ice core. *Clim. Past* 8, 1239–1255. <http://dx.doi.org/10.5194/cp-8-1239-2012>.
- Pausata, F.S.R., Battisti, D.S., Nisancioglu, K.H., Bitz, C.M., 2011. Chinese stalagmite d₁₈O controlled by changes in the Indian monsoon during a simulated Heinrich event. *Nat. Geosci.* 4, 474–480.
- Pedro, J.B., Rasmussen, S.O., van Ommen, T.D., 2012. Tightened constraints on the time-lag between Antarctic temperature and CO₂ during the last deglaciation. *Clim. Past* 8, 1213–1221. <http://dx.doi.org/10.5194/cp-8-1213-2012>.
- Pol, K., Debret, M., Masson-Delmotte, V., Capron, E., Cattani, O., Dreyfus, G., Falourd, S., Johnsen, S., Jouzel, J., Landais, A., Minster, B., Stenni, B., 2011. Links between MIS 11 millennial to sub-millennial climate variability and long term trends as revealed by new high resolution EPICA Dome C deuterium data – a comparison with the Holocene. *Clim. Past* 7, 437–450. <http://dx.doi.org/10.5194/cp-7-437-2011>.
- Pol, K., Masson-Delmotte, V., Cattani, O., Debret, M., Falourd, S., Jouzel, J., Landais, A., Minster, B., Mudelsee, M., Schulz, M., Stenni, B., 2014. Climate variability features of the last interglacial in the East Antarctic EPICA Dome C ice core. *Geophys. Res. Lett.* 41 (11), 4004–4012. <http://dx.doi.org/10.1002/2014GL059561>.
- Raisbeck, G.M., Yiou, F., Jouzel, J., Stocker, T.F., 2007. Direct north-south synchronization of abrupt climate change record in ice cores using Beryllium 10. *Clim. Past* 3, 541–547. <http://dx.doi.org/10.5194/cp-3-541-2007>.
- Rasmussen, S.O., Abbott, P.M., Blunier, T., Bourne, A.J., Brook, E., Buchardt, S.L., Buizert, C., Chappellaz, J., Clausen, H.B., Cook, E., Dahl-Jensen, D., Davies, S.M., Guillevic, M., Kipfstuhl, S., Laepple, T., Seierstad, I.K., Severinghaus, J.P., Steffensen, J.P., Stowasser, C., Svensson, A., Vallelonga, P., Vinther, B.M., Wilhelms, F., Winstrup, M., 2013. A first chronology for the North Greenland Eemian Ice Drilling (NEEM) ice core. *Clim. Past* 9, 2713–2730. <http://dx.doi.org/10.5194/cp-9-2713-2013>.
- Rind, D., Russell, G.L., Schmidt, G.A., Sheth, S., Collins, D., Demenocal, P., Teller, J., 2001. Effects of glacial meltwater in the GISS Coupled Atmosphere-Ocean Model: part II: a bi-polar seesaw in Atlantic Deep Water production. *J. Geophys. Res.* 106, 27355–27366. <http://dx.doi.org/10.1029/2001JD000954>.
- Roberts, W.G.H., Valdes, P.J., Payne, A.J., 2014. Topography's crucial role in Heinrich events. *PNAS* 111 (47), 16688–16693. <http://dx.doi.org/10.1073/pnas.1414882111>.

- Roche, D.M., Wiersma, A.P., Renssen, H., 2010. A systematic study of the impact of freshwater pulses with respect to different geographical locations. *Clim. Dyn.* 34, 997–1013.
- Rosen, J.L., Brook, E.J., Severinghaus, J.P., Blunier, T., Mitchell, L.E., Lee, J.E., Edwards, J.S., Gkinis, V., 2014. An ice core record of near-synchronous global climate changes at the Bolling transition. *Nat. Geosci.* 7, 459–463. <http://dx.doi.org/10.1038/ngeo2147>.
- Ruth, U., Barnola, J.-M., Beer, J., Bigler, M., Blunier, T., Castellano, E., Fischer, H., Fundel, F., Huybrechts, P., Kaufmann, P., Kipfstuhl, S., Lambrecht, A., Morganti, A., Oerter, H., Parrenin, F., Rybak, O., Severi, M., Udisti, R., Wilhelms, F., Wolff, E., 2007. “EDML1”: a chronology for the EPICA deep ice core from Dronning Maud Land, Antarctica, over the last 150 000 years. *Clim. Past* 3, 475–484. <http://dx.doi.org/10.5194/cp-3-475-2007>.
- Sanchez Goni, M.F., Landais, A., Fletcher, W.J., Naughton, F., Desprat, S., Duprat, J., 2008. Contrasting impacts of Dansgaard-Oeschger events over a western European latitudinal transect modulated by orbital parameters. *Quat. Sci. Rev.* 27, 1136–1151.
- Sanchez-Goni, M.F., Harrison, S.P., 2010. Millennial-scale climate variability and vegetation changes during the Last Glacial: concepts and terminology. *Quat. Sci. Rev.* 29, 2823–2827.
- Sarchilli, C., Frezzotti, M., Ruti, P.M., 2011. Snow precipitation at four ice core sites in East Antarctica: provenance, seasonality and blocking factors. *Clim. Dyn.* 37, 2107–2125. <http://dx.doi.org/10.1007/s00382-010-0946-4>.
- Schilt, A., Baumgartner, M., Blunier, T., Schwander, J., Spahni, R., Fischer, H., Stocker, T.F., 2010. Glacial-interglacial and millennial-scale variations in the atmospheric nitrous oxide concentration during the last 800,000 years. *Quat. Sci. Rev.* 29 (1–2), 182–192.
- Schüpbach, S., Federer, U., Bigler, M., Fischer, H., Stocker, T.F., 2011. A refined TALDICE-1a age scale from 55 to 112 ka before present for the Talos Dome ice core based on high-resolution methane measurements. *Clim. Past* 7, 1001–1009. <http://dx.doi.org/10.5194/cp-7-1001-2011>.
- Schüpbach, S., Federer, U., Kaufmann, P.R., Albani, S., Barbante, C., Stocker, T.F., Fischer, H., 2013. High-resolution mineral dust and sea ice proxy records from the Talos Dome ice core. *Clim. Past* 9, 2789–2807.
- Seidov, D., Stouffer, R.J., Haupt, B.J., 2005. Is there a simple bi-polar seesaw? *Global Planet. Change* 49, 19–27.
- Severi, M., Becagli, S., Castellano, E., Morganti, A., Traversi, R., Udisti, R., Ruth, U., Fischer, H., Huybrechts, P., Wolff, E., Parrenin, F., Kaufmann, P., Lambert, F., Steffensen, J.P., 2007. Synchronisation of the EDML and EDC ice cores for the last 52 kyr by volcanic signature matching. *Clim. Past* 3, 367–374. <http://dx.doi.org/10.5194/cp-3-367-2007>.
- Severi, M., Udisti, R., Becagli, S., Stenni, B., Traversi, R., 2012. Volcanic synchronisation of the EPICA-DC and TALDICE ice cores for the last 42 kyr BP. *Clim. Past* 8, 509–517. <http://dx.doi.org/10.5194/cp-8-509-2012>.
- Severinghaus, J.P., Brook, E.J., 1999. Abrupt climate change at the end of the last glacial period inferred from trapped air in polar ice. *Science* 286, 930–934. <http://dx.doi.org/10.1126/science.286.5441.930>.
- Severinghaus, J.P., Sowers, T., Brook, E.J., Alley, R.B., Bender, M.L., 1998. Timing of abrupt climate change at the end of the Younger Dryas interval from thermally fractionated gases in polar ice. *Nature* 391, 141–146. <http://dx.doi.org/10.1038/34346>.
- Shaffer, G., Olsen, S.M., Bjerrum, C.J., 2004. Ocean subsurface warming as a mechanism for coupling Dansgaard-Oeschger climate cycles and ice-rafting events. *Geophys. Res. Lett.* 31, L24202. <http://dx.doi.org/10.1029/2004GL020968>.
- Singer, B.S., Guillou, H., Jicha, B.R., Laj, C., Kissel, C., Beard, B.L., Johnson, C.M., 2009. ⁴⁰Ar/³⁹Ar, K–Ar and ²³⁰Th–²³⁸U dating of the Laschamp excursion: a radioisotopic tie-point for ice core and climate chronologies. *Earth Planet. Sci. Lett.* 286 (1–2), 80–88.
- Smith, D.E., Harrison, S., Firth, C.R., Jordan, J.T., 2011. The early Holocene sea level rise. *Quat. Sci. Rev.* 30, 1846–1860.
- Stenni, B., Masson-Delmotte, V., Selmo, E., Oerter, H., Meyer, H., Roethlisberger, R., Jouzel, J., Cattani, O., Falourd, S., Fischer, H., Hoffmann, G., Iacumin, P., Johnsen, S.J., Minster, B., Udisti, R., 2010. The deuterium excess records of EPICA Dome C and Dronning Maud Land ice cores (East Antarctica). *Quat. Sci. Rev.* 29 (1–2), 146–159.
- Stocker, T.F., Johnsen, S.J., 2003. A minimum thermodynamic model for the bipolar seesaw. *Paleoceanography* 18, 1087. <http://dx.doi.org/10.1029/2003PA000920>.
- Stouffer, R.J., Yin, J., Gregory, J.M., Dixon, K.W., Spelman, M.J., Hurlin, W., Weaver, A.J., Eby, M., Flato, G.M., Hasumi, H., Hu, A., Jungclauss, J.H., Kammenkovich, I.J., Levermann, A., Montoya, M., Murakami, S., Nawrath, S., Oka, A., Peltier, W.R., Robitaille, D.Y., Sokolov, A., Vettoretti, G., Weber, S.L., 2006. Investigating the causes of the response of the thermohaline circulation to past and future climate changes. *J. Clim.* 19, 1365–1387. <http://dx.doi.org/10.1175/JCLI3689.1>.
- Stouffer, R.J., Seidov, D., Haupt, B.J., 2007. Climate response to external sources of freshwater: North Atlantic versus the Southern Ocean. *J. Clim.* 20 (3) <http://dx.doi.org/10.1175/JCLI4015.1>.
- Svensson, A., Andersen, K.K., Bigler, M., Clausen, H.B., Dahl-Jensen, D., Davies, S.M., Johnsen, S.J., Muscheler, R., Parrenin, F., Rasmussen, S.O., Röthlisberger, R., Seierstad, I., Steffensen, J.P., Vinther, B.M., 2008. A 60 000 year Greenland stratigraphic ice core chronology. *Clim. Past* 4, 47–57. <http://dx.doi.org/10.5194/cp-4-47-2008>.
- Svensson, A., Bigler, M., Blunier, T., Clausen, H.B., Dahl-Jensen, D., Fischer, H., Fujita, S., Goto-Azuma, K., Johnsen, S.J., Kawamura, K., Kipfstuhl, S., Kohno, M., Parrenin, F., Popp, T., Rasmussen, S.O., Schwander, J., Seierstad, I., Severi, M., Steffensen, J.P., Udisti, R., Uemura, R., Vallelonga, P., Vinther, B.M., Wegner, A., Wilhelms, F., Winstrup, M., 2013. Direct linking of Greenland and Antarctic ice cores at the Toba eruption (74 ka BP). *Clim. Past* 9, 749–766. <http://dx.doi.org/10.5194/cp-9-749-2013>.
- Swingedouw, D., Fichet, T., Huybrechts, P., Driesschaert, M., Goosse, H., Loutre, M.F., 2008. Antarctic ice-sheet melting provides negative feedbacks on future global warming. *Geophys. Res. Lett.* 35, Art. No L17705.
- Swingedouw, D., Mignot, J., Braconnot, P., Mosquet, E., Kageyama, M., Alkama, R., 2009. Impact of freshwater release in the North Atlantic under different climate conditions in an OAGCM. *J. Clim.* 22, 6377–6403.
- Timmermann, A., Menviel, L., Okumura, Y., Schilla, A., Merkel, U., Timm, O., Hu, A., Otto-Bliesner, B., Schulz, M., 2010. Towards a quantitative understanding of millennial-scale Antarctic Warming events. *Quat. Sci. Rev.* 29, 74–85.
- Udisti, R., Becagli, S., Castellano, E., Delmonte, B., Jouzel, J., Petit, J.-R., Schwander, J., Stenni, B., Wolff, E.W., 2004. Stratigraphic correlations between the EPICA-Dome C and Vostok ice cores showing the relative variations of snow accumulation over the past 45 kyr. *J. Geophys. Res.* 109, D08101. <http://dx.doi.org/10.1029/2003jd004180>.
- Veres, D., Bazin, L., Landais, A., Toyé Mahamadou Kele, H., Lemieux-Dudon, B., Parrenin, F., Martinerie, P., Blayo, E., Blunier, T., Capron, E., Chappellaz, J., Rasmussen, S.O., Severi, M., Svensson, A., Vinther, B., Wolff, E.W., 2013. The Antarctic ice core chronology (AICC2012): an optimized multi-parameter and multi-site dating approach for the last 120 thousand years. *Clim. Past* 9, 1733–1748. <http://dx.doi.org/10.5194/cp-9-1733-2013>.
- Vimeux, F., Masson, V., Jouzel, J., Stievenard, M., Petit, J.-R., 1999. Glacial-interglacial changes in ocean surface conditions in the Southern Hemisphere. *Nature* 398, 410–413.
- Voelker, A.H.L., 2002. Global distribution of centennial-scale records for Marine Isotope Stage (MIS) 3: a database. *Quat. Sci. Rev.* 21, 1185–1212.
- Weaver, A.J., Saenko, O.A., Clark, P.U., Mitrovica, J.X., 2003. Meltwater pulse 1A from Antarctica as a trigger of the Bolling-Allerød warm interval. *Science* 299, 1709–1713.
- Wegner, A., Gabrielli, P., Wilhelms-Dick, D., Ruth, U., Kriews, M., De Deckker, P., Barbante, C., Cozzi, G., Delmonte, B., Fischer, H., 2012. Change in dust variability in the Atlantic sector of Antarctica at the end of the last deglaciation. *Clim. Past* 8, 135–147. <http://dx.doi.org/10.5194/cp-8-135-2012>.
- Welander, P., 1982. A simple heat-salt oscillator. *Dyn. Atmos. Ocean* 6, 233–242.
- Werner, M., Heimann, M., Hoffmann, G., 2001. Isotopic composition and origin of polar precipitation in present and glacial climate simulations. *Tellus B* 53 (1).
- Wunsch, C., 2006. Abrupt climate change: an alternative view. *Quat. Res.* 65, 191–203.
- Zhang, X., Lohmann, G., Knorr, G., Purcell, C., 2014. Abrupt glacial climate shifts controlled by ice sheet changes. *Nature*. <http://dx.doi.org/10.1038/nature13592> (online 13 August 2014).